NAVAL POSTGRADUATE SCHOOL
Monterey, California

THESIS

OPTIMIZATION OF MAS AND MODIS POLAR OCEAN CLOUD MASK

by

Sean P. Memmen

June 2000

Thesis Advisor: Philip A. Durkee
Second Reader: Peter S. Guest

Approved for public release; distribution is unlimited.

REPORT DOCUMENTATION PAGE			Form Approved OMB No. 0704-0188
Public reporting burden for this collection of information is estimated to average 1 hour per response, including the time for reviewing instruction, searching existing data sources, gathering and maintaining the data needed, and completing and reviewing the collection of information. Send comments regarding this burden estimate or any other aspect of this collection of information, including suggestions for reducing this burden, to Washington headquarters Services, Directorate for Information Operations and Reports, 1215 Jefferson Davis Highway, Suite 1204, Arlington, VA 22202-4302, and to the Office of Management and Budget, Paperwork Reduction Project (0704-0188) Washington DC 20503.			
1. AGENCY USE ONLY *(Leave blank)*	**2. REPORT DATE** June 2000	**3. REPORT TYPE AND DATES COVERED** Master's Thesis	
4. TITLE AND SUBTITLE: Optimization of MAS and MODIS Polar Ocean Cloud Mask			**5. FUNDING NUMBERS**
6. AUTHOR(S) Sean P. Memmen			
7. PERFORMING ORGANIZATION NAME(S) AND ADDRESS(ES) Naval Postgraduate School Monterey, CA 93943-5000			**8. PERFORMING ORGANIZATION REPORT NUMBER**
9. SPONSORING / MONITORING AGENCY NAME(S) AND ADDRESS(ES) N/A			**10. SPONSORING / MONITORING AGENCY REPORT NUMBER**
11. SUPPLEMENTARY NOTES The views expressed in this thesis are those of the author and do not reflect the official policy or position of the Department of Defense or the U.S. Government.			
12a. DISTRIBUTION / AVAILABILITY STATEMENT Approved for public release; distribution unlimited			**12b. DISTRIBUTION CODE**

13. ABSTRACT ***(maximum 200 words)*** With the reduction of funding for sea ice reconnaissance flights, the National/Naval Ice Center needs to capitalize on the improvements in satellite technology. Imaging sensors such as AVHRR, DMSP/OLS, SSM/I and RADARSAT have been used to detect the presence of sea ice, but with the exception of SSM/I and RADARSAT, clouds are a major obstacle to viewing the surface. With NASA's development of the Moderate-resolution Imaging Spectroradiometer (MODIS) and MODIS Airborne Simulator (MAS), there is finally a sensor capable of using multi-spectral techniques to detect the presence of clouds.

A group at the Space Science and Engineering Center (SSEC), University of Wisconsin – Madison lead by Dr. Steve Ackerman has developed a mask for MAS/MODIS. The technique determines a level of confidence that a given pixel is clear based on a series of multi-spectral tests. By combining the confidence level from all tests, it is possible to detect the presence of clouds at different altitudes in the atmosphere. Based on the Ackerman et al. (1997) scheme, threshold optimizations were made on the $T_B(11\mu m)$ and $T_B(3.9\mu m)$ - $T_B(11\mu m)$ tests, while the $T_B(11\mu m)$ - $T_B(12\mu m)$ test was removed. These are daytime modifications based on analysis of several MAS and a limited number of MODIS cases.

From subjective analysis, the modifications greatly improved the detection of clouds over cold polar oceans where sub-pixel ice may be present or water temperatures might falsely indicate clouds. The number of *Cloudy* pixels (≤ 0.66 clear confidence level) for a given scene was increased 12.1% on average for MAS cases. The NPS cloud mask also classified two times more *Probably Clear* and *Undecided* pixels than the original mask due to greater sensitivity to thin, small clouds.

14. SUBJECT TERMS Moderate Resolution Imaging Spectroradiometer (MODIS), MODIS Airborne Simulator (MAS), Terra Satellite, Cloud Mask, Sea Ice			**15. NUMBER OF PAGES**
			16. PRICE CODE
17. SECURITY CLASSIFICATION OF REPORT Unclassified	**18. SECURITY CLASSIFICATION OF THIS PAGE** Unclassified	**19. SECURITY CLASSIFICATION OF ABSTRACT** Unclassified	**20. LIMITATION OF ABSTRACT** UL

NSN 7540-01-280-5500

Standard Form 298 (Rev. 2-89)
Prescribed by ANSI Std. 239-18

THIS PAGE INTENTIONALLY LEFT BLANK

Approved for public release; distribution is unlimited.

OPTIMIZATION OF MAS AND MODIS POLAR OCEAN CLOUD MASK

Sean P. Memmen
Lieutenant, United States Navy
B.S., State University of New York, Maritime College, 1992

Submitted in partial fulfillment of the
requirements for the degree of

**MASTER OF SCIENCE IN METEOROLOGY
AND PHYSICAL OCEANOGRAPHY**

from the

**NAVAL POSTGRADUATE SCHOOL
June 2000**

Author: 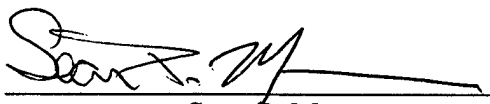
Sean P. Memmen

Approved by: 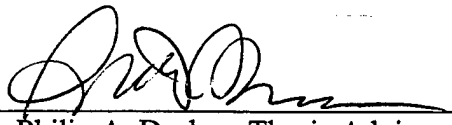
Philip A. Durkee, Thesis Advisor


Peter S. Guest, Second Reader

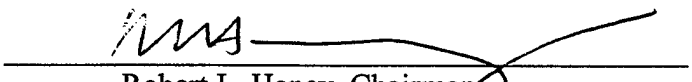
Robert L. Haney, Chairman
Department of Meteorology

THIS PAGE INTENTIONALLY LEFT BLANK

ABSTRACT

With the reduction of funding for sea ice reconnaissance flights, the National/Naval Ice Center needs to capitalize on the improvements in satellite technology. Imaging sensors such as AVHRR, DMSP/OLS, SSM/I and RADARSAT are used to detect the presence of sea ice, but with the exception of SSM/I and RADARSAT, clouds are a major obstacle to viewing the surface. With NASA's development of the Moderate-resolution Imaging Spectroradiometer (MODIS) and MODIS Airborne Simulator (MAS), there is finally a sensor capable of using multi-spectral techniques to detect the presence of clouds.

A group at the Space Science and Engineering Center (SSEC), University of Wisconsin – Madison lead by Dr. Steve Ackerman has developed a cloud mask for MAS/MODIS. The technique determines a level of confidence that a given pixel is clear based on a series of multi-spectral tests. By combining the confidence level from all tests, it is possible to detect the presence of clouds at different altitudes in the atmosphere. Threshold optimizations are described in this thesis for the $T_B(11\mu m)$ and $T_B(3.9\mu m)$ - $T_B(11\mu m)$ tests from Ackerman et al. (1997). In addition, the $T_B(11\mu m)$ - $T_B(12\mu m)$ test is removed. These modifications are based on daytime analysis of several MAS cases and a limited number of MODIS cases.

Subjective analysis shows the modifications greatly improve the detection of clouds over cold polar oceans where sub-pixel ice may be present or water temperatures might falsely indicate clouds. The number of *Cloudy* pixels (≤ 0.66 clear confidence level) for a given scene was increased 12.1% on average for MAS cases. The NPS cloud mask also classified two times more *Probably Clear* and *Undecided* pixels than the original mask due to greater sensitivity to thin, small clouds.

THIS PAGE INTENTIONALLY LEFT BLANK

TABLE OF CONTENTS

LIST OF FIGURES

LIST OF TABLES

THIS PAGE INTENTIONALLY LEFT BLANK

ACKNOWLEDGMENTS

The author wishes to thank Professor Philip A. Durkee for his guidance, insight, support and assistance throughout the course of this research. He truly made the thesis process an enjoyable learning experience. Research Associate Professor Peter S. Guest is thanked for his careful review of the manuscript and for his helpful comments. Much appreciation is extended to Robert L. Creasey of the Naval Postgraduate School's Interactive Digital Environmental Analysis (IDEAL) Laboratory for his assistance in computer processing and software support. Kurt Nielsen is thanked for the many hours of help in the Remote Sensing Laboratory. The author also wishes to thank the staff at the Space Science and Engineering Center at the University of Wisconsin – Madison for all their assistance with the cloud mask algorithm. Of special note are, Liam E. Gumley for his SHARP and MODVIS programs which allowed for the visual display of MODIS and MAS imagery and Kathy Strabala for her guidance in understanding the algorithm code. Jeff Key of NOAA/NESDIS at the University of Wisconsin – Madison for his hospitality during my visit to the University of Wisconsin – Madison. In addition, Dave Benner, Cheryl Bertoia and Paul Seymour at the National/Naval Ice Center are thanked for their funding and guidance in operational sea ice analyses. Finally, a special loving thanks to the author's wife Tara and daughter Kaitlin whose steadfast patience and understanding throughout this effort have paid incalculable dividends.

THIS PAGE INTENTIONALLY LEFT BLANK

INTRODUCTION

A. MOTIVATION

With the reduction of funding for sea ice reconnaissance flights, manned polar observation stations, and polar *in situ* measurements, the National/Naval Ice Center (NIC) needs to capitalize on the latest advances in remote sensing. Clouds can be characterized by either their brightness temperature or reflectance characteristics. Previous cloud masks used simple combinations of visible and IR wavelengths to detect the presence of clouds. Cloud detection is difficult in polar ocean regions where sea ice may have the same brightness temperature and/or reflectance of the surrounding clouds. Detection becomes further complicated when clouds are thin along their edges and are almost indistinguishable from the sea ice.

The Moderate Resolution Imaging Spectroradiometer (MODIS) and the MODIS Airborne Simulator (MAS) provide an opportunity for multi-spectral cloud detection approaches using many more wavelengths than previously available. Multi-spectral cloud detection will take advantage of the many differences in the spectral properties of sea ice and clouds. As a result, future automated sea ice analysis algorithms will more correctly identify sea ice properties with minimal cloud contamination.

B. HISTORY

Operational analysis of sea ice using remote sensing assets date back to the 1970's. Analysts manually analyzed sea ice in imagery with grease pencils and eventually transferred the analyses to paper charts. In the early 1990's, on-screen sea ice analysis became possible due to increased computer power and products were

disseminated via the World Wide Web. The future objective of operational sea ice analysis is an automated process with minimal manual intervention. Automated analysis requires a cloud mask that is sensitive to the unique conditions present in polar ocean regions.

Satellite sensors are available that can penetrate clouds to derive surface information without the need of a cloud mask. One is a passive microwave sensor called Special Sensor Microwave Imager (SSM/I) on the Defense Meteorological Satellite Program (DMSP). SSM/I techniques usually use 85GHz imagery to identify sea ice and cloud liquid water content. SSM/I is not the perfect ice detection instrument. Microwave techniques currently provide low-resolution observations (ca. 25km) and have difficulty identifying sea ice concentrations when water pools on top of the sea ice. A second active technique uses the Synthetic Aperture Radar (SAR). For example RADARSAT uses a 5.3GHz radar to penetrate clouds and view the surface. SAR is an ideal tool for operational sea ice analysis but is restrictive due to the cost per scene to the U.S. Government.

C. OBJECTIVE

The objective of this thesis is to optimize a cloud mask for MODIS that is optimized for the polar ocean region and used by NIC and other polar scientists. The work described here is based on a cloud mask that was originally developed by the Space Science and Engineering Center at the University of Wisconsin - Madison. The optimized cloud mask will assist in the operational sea ice analysis by identifying clouds that might be mistaken as sea ice or their shadows mistaken as leads. The ultimate goal is the initialization of an automated sea ice analysis algorithm.

D. ORGANIZATION

Chapter II outlines background information about the MAS/MODIS cloud mask. Chapter III describes the methodology for optimizing the MAS/MODIS Cloud mask. Chapter IV shows MAS examples of the NPS cloud mask adjustments. Finally, Chapter V shows a MODIS example of the NPS cloud mask and Chapter VI outlines the conclusions of this thesis and offers recommendations for further studies.

THIS PAGE INTENTIONALLY LEFT BLANK

II. BACKGROUND INFORMATION

A. PLATFORMS AND SENSORS

Two platform/sensor packages are employed by the cloud mask algorithm. First is the ER-2 and MAS research sensor, which is used to evaluate channel properties. Second is the Terra Satellite and MODIS operational space-borne sensor.

1. ER-2 and MAS

MAS is a modified Daedalus Wildfire scanning spectrometer that is flown on a NASA ER-2 aircraft. It has been used in many experiments including WINCE (January – February 1997) and FIRE/ACE (May – June 1998). It provides 50 band, 50m resolution from 20km flight altitude in 50 spectral bands range from 0.523μm to 14.383μm wavelengths (Table 2-1). Band spectral ranges can change depending on the experiment.

2. Terra Satellite and MODIS

The Terra satellite, formally AM-1, is the flagship of the Earth Observing System (EOS). EOS is a major program under the National Aeronautics and Space Administration's (NASA) Earth Science Enterprise (ESE) with a primary mission to observe the Earth's surface. Terra was launched from the Western Test Range, Vandenburg Air Force Base, California on December 18, 1999 at 13:57 EST (Herring, 2000). It is in a 10:30am local equator crossing, descending, Sun synchronous orbit in attempt to maximize the view of the surface while minimizing cloud cover. The orbit will be adjusted to ensure a complete surface coverage every 16 days with a life span of 6 years (NASA, 1999a).

Table 2.1. MAS Instrument/Platform Specifications

Platform	NASA ER-2 Aircraft	**Swath Width**	73.25 km or 22.9 miles (at 20 km altitude)
Ground Speed	400 kts (206 m/s)	**Total Field of View**	85.92°
Pixel Spatial Resolution	50 m (at 20 km)	**Instantaneous Field of view**	2.5 milliradians
Pixel per Scan Line	716 (roll corrected)	**Roll Correction**	+/- 3.5°
Scan Rate	6.25 scans/second	**Data Channels**	50 channels via digital recorded

Spectral Bands			
Band	**Bandwidth**	**Band**	**Bandwidth**
1	0.523 – 0.569	26	2.875 – 3.039
2	0.627 – 0.68	27	3.031 – 3.195
3	0.679 – 0.721	28	3.202 – 3.358
4	0.72 – 0.762	29	3.338 – 3.507
5	0.761 – 0.802	30	3.511 – 3.668
6	0.802 – 0.844	31	3.669 – 3.819
7	0.844 – 0.886	32	3.819 – 3.986
8	0.888 – 0.922	33	3.979 – 4.132
9	0.921 – 0.967	34	4.126 – 4.288
10	1.595 – 1.65	35	4.288 – 4.435
11	1.652 – 1.705	36	4.439 – 4.594
12	1.706 – 1.757	37	4.585 – 4.748
13	1.759 – 1.812	38	4.745 – 4.901
14	1.813 – 1.863	39	4.897 – 5.047
15	1.863 – 1.914	40	5.046 –5.203
16	1.914 - .1963	41	5.205 – 5.362
17	1.964 – 2.013	42	8.386 – 8.822
18	2.014 – 2.064	43	9.484 – 10.101
19	2.066 – 2.113	44	10.3 – 10.794
20	2.114 – 2.162	45	10.746 – 11.289
21	2.163 – 2.21	46	11.736 – 12.185
22	2.211 – 2.261	47	12.651 – 13.47
23	2.262 – 2.31	48	12.998 – 13.47
24	2.312 – 2.36	49	13.421 – 14.021
25	2.361 – 2.41	50	13.96 – 14.383

One of the five instruments aboard TERRA is MODIS. It has 36 bands ranging from 0.4μm to 14.4μm wavelength. The bands are designed to observe land and ocean temperatures, land surface coverage, aerosols, water vapor, temperature profiles, and fires. Table 2-2 lists the various spectral bands, their associated spatial resolutions and primary use.

B. MAS/MODIS ARCTIC CLOUD MASK

The MAS/MODIS Cloud Mask is described in the algorithm theoretical basic document (ATBD) (Ackerman et al., 1997). The physical rationale and detail specifications of the cloud mask are documented in the ATBD. This thesis will only describe the important factors that effect cloud detection in polar ocean regions.

Figure 2.1 shows MAS and MODIS bands overlaid on the transmittance properties for ozone, water vapor and carbon dioxide for a mid-latitude summer atmosphere calculated by MODTRAN 3.5 (Acharya et al., 1993). In general, cloud and surface observations are made in spectral regions with minimal atmospheric absorption. However, absorption bands can be used to limit the radiance from lower altitudes. This can help identify upper-level clouds.

1. General overview of the Cloud Mask

It is evident that the MAS and MODIS sensors have much in common in the exploitation of transmission and absorption features. In some cases they used different wavelengths to achieve the same result. As an example, MAS uses a 1.88μm band to exploit low and mid level strong water vapor absorption to highlight the presence of high,

Table 2.2. MODIS Characteristics (NASA, 1999b)

Primary Use	Band	Bandwidth	Spatial Resolution (Nadir)
Land/Cloud Boundaries	1	0.620 – 0.670 μm	250 m
	2	0.841 – 0.876 μm	250 m
Land/Cloud Properties	3	0.459 – 0.479 μm	500 m
	4	0.545 – 0.565 μm	500 m
	5	1.230 – 1.250 μm	500 m
	6	1.628 – 1.652 μm	500 m
	7	2.105 – 2.155 μm	500 m
Ocean Color/ Phytoplankton/ Biogeochemistry	8	0.405 – 0.420 μm	1000 m
	9	0.438 – 0.448 μm	1000 m
	10	0.483 – 0.493 μm	1000 m
	11	0.526 – 0.536 μm	1000 m
	12	0.546 – 0.556 μm	1000 m
	13	0.662 – 0.672 μm	1000 m
	14	0.673 – 0.683 μm	1000 m
	15	0.743 – 0.753 μm	1000 m
	16	0.862 – 0.877 μm	1000 m
Atmospheric Water Vapor	17	0.890 – 0.920 μm	1000 m
	18	0.931 – 0.941 μm	1000 m
	19	0.915 – 0.965 μm	1000 m
Surface/Cloud Temperature	20	3.660 – 3.840 μm	1000 m
	21	3.929 – 3.989 μm	1000 m
	22	3.929 – 3.989 μm	1000 m
	23	4.020 – 4.080 μm	1000 m
Atmospheric Temperature	24	4.433 – 4.498 μm	1000 m
	25	4.482 – 4.549 μm	1000 m
Cirrus Clouds	26	1.360 – 1.390 μm	1000 m
Water Vapor	27	6.535 – 6.895 μm	1000 m
	28	7.175 – 7.475 μm	1000 m
	29	8.400 – 8.700 μm	1000 m
Ozone	30	9.580 – 9.880 μm	1000 m
Surface/Cloud Temperature	31	10.780 – 11.280 μm	1000 m
	32	11.770 – 12.270 μm	1000 m
Cloud Top Altitude	33	13.185 – 13.485 μm	1000 m
	34	13.485 – 13.785 μm	1000 m
	35	13.785 – 14.085 μm	1000 m
	36	14.085 – 14.385 μm	1000 m

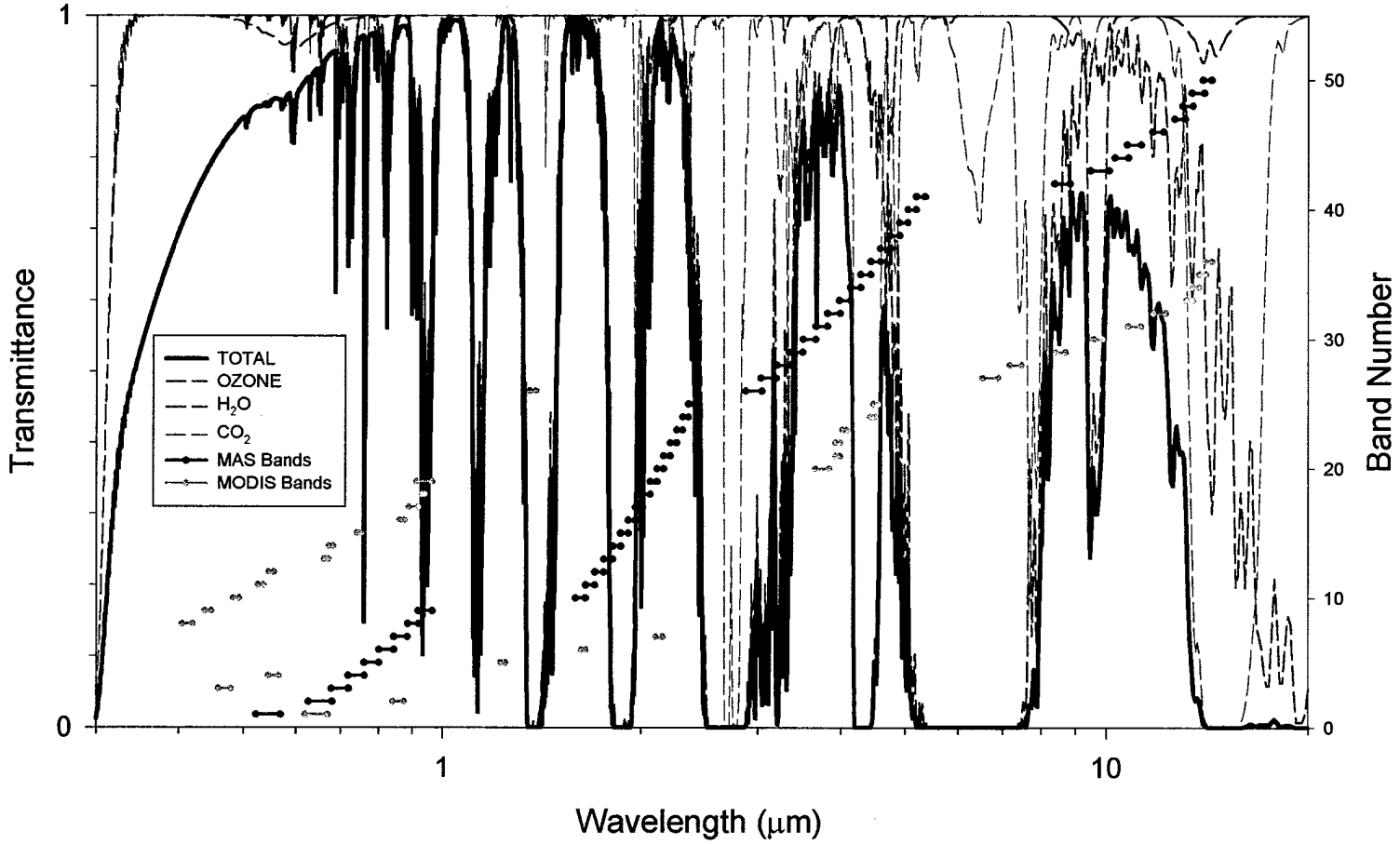

Figure 2.1. MAS/MODIS bands - frequency relationship where these instruments exploit the various atmospheric properties to obtain information about the atmosphere. Overlaid are the transmittance properties for ozone, water vapor and carbon dioxide

thin cirrus clouds. To accomplish the same task, MODIS uses the water vapor absorption band at 1.38μm.

There are five major groups of multi spectral tests in the mask. Each group of tests are designed to detect common cloud features ranging from low clouds to high cirrus clouds. The number of tests within a group and the number of groups used in a particular case vary depending on the time of day, the ecosystem, presence of snow or sea ice, amount of perceptible water, and several others. Once an individual pixel's characteristics have been described (e.g. daytime, ocean, polar, ice), tests within various groups will be preformed along with specific thresholds for that pixel's characteristics. All tests within a group and all groups have the same weight as any other test or group used for a pixel.

a. Calculation of Confidence

Ackerman et al. (1997) developed a simple linear scaling of thresholds. This technique allows for a degree of uncertainty to be included in each test. Figure 2.2 depicts the linear function used by the cloud mask. There are three points; alpha (α) - any value below this point is considered cloudy, beta (β) - this is the 50% clear confidence value (the pixel can be either clear or cloudy) and gamma (γ) - any value above this point is considered clear. Each test within a group is given a value between 0 and 1 depending on its threshold. A value of 0 is an indication of a high probability of cloud, while a value of 1 is an indication of a high probability of a clear condition. The lowest confidence value from the tests within a group becomes the value for the over all group.

The overall clear confidence value for the pixel, Q, is computed for the pixel as the N^{th} root the product of group confidence values:

$$Q = \sqrt[N]{\prod_{i=1}^{N} G_i}\,, \tag{2-1}$$

where G_i is the value for a group and N is the number of groups used in the test. This calculation is conservative in the estimate of a clear sky condition and will err on the cloudy side for any given pixel. For example, if a pixel were in a daytime, ocean, polar, sea ice location, the cloud mask would use four groups for the test. Confidence values for the four individual groups might be 0.82, 0.66, 1, and 1. Therefore the over all confidence would be $[(0.82)(0.66)(1)(1)]^{1/4} = 0.86$ for that pixel. Table 2.3 shows Q values for the four confidence levels. The pixel in this example would be assigned as *Undecided* classification.

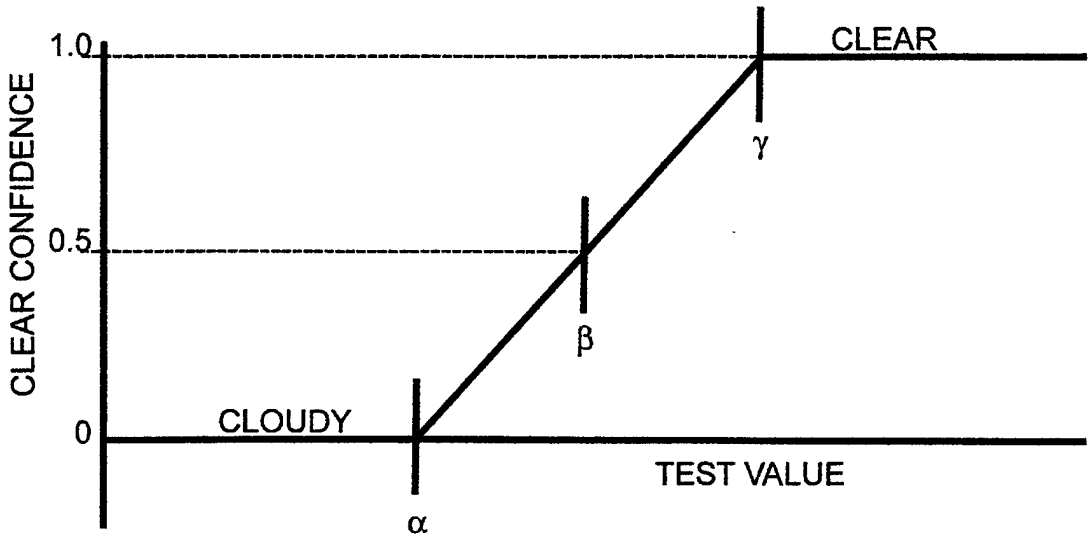

Figure 2.2. Clear confidence level linear function used by the cloud mask.

Table 2.3. Confidence Values

Confidence	Q
Undecided	$Q > 0.66$
Cloudy or Obstructed	$Q \leq 0.66$

2. Inputs

The cloud mask requires some information about the scene before it can determine if a pixel is clear or not. These inputs determine the number of groups and the number of tests that will be preformed within each group. Some of the variables that are important for the polar ocean portion of the mask are day/night, ecosystem, and sea ice detection.

a. Day/Night

The day/night calculation is based on the solar zenith sun angle (θ). When $\theta > 85°$ it is considered day time (Ackerman et al., 1997).

b. Ecosystem

The ecosystem is determined by the pixel's location within various index files and may be manually selected. They are:

1. Global USGS 1 km resolution land/sea tag
2. Loveland 1 km resolution N. American ecosystem
3. 10 minute resolution global Olson ecosystem
4. Global Loveland 1 km resolution Olson ecosystem

For the MAS cases, the Global Loveland 1 km resolution Olson ecosystem file was used to identify the ecosystem. The ecosystem is identified as either being desert, land, coast or ocean.

c. Sea Ice Detection

There are challenges to overcome when it comes to the detection of sea ice. First, sea ice detection is difficult when there are low clouds in the scene due to their similar radiance and thermal signatures. Second, relatively thin sea ice detection is difficult because polar ocean waters might have similar radiance values.

The MODIS cloud mask has two ways to detect the presence of sea ice. First, Special Sensor Microwave Imager (SSM/I) analysis at 25km resolution, available from either the National Center for Environmental Predictions (NCEP) or the National Snow and Ice Data Center (NSIDC), is used to identify the presence of sea ice. The inputs from NCEP and NSIDC are given equal weight in the mask for the determination of sea ice extent. Unfortunilty, SSM/I has diffuculty in the summer when liquid water pools on top of sea ice and might incorrectly indicate an open water condition.

Second, an internal means for idenfitying sea ice was developed by Hall et al., (1998) (herafter referred to the Hall Test) and implimented in the mask in an attempt to determine the pixel-scale extent in sea ice. In the Hall Test, when the brightness temperature at 11μm, $T_B(11\mu m)$, is less than 280°K, the surface is assumed to be cold enough to have snow or sea ice present. The difference between snow or sea ice depends on whether the ecosystem is either land/coastal or ocean. Next, the Normalized Difference Snow Index (NDSI) test detects sea ice when its thickness is greater than 10cm. This works because sea ice absorbs 1.62μm wavelength radiance. Therefore, when sea ice is present, visible reflectance, $\rho_{0.55\mu m}$, will be greater than 1.62μm reflectance, $\rho_{1.62\mu m}$. In addition, sea ice has a high reflectance at 0.88μm wavelength

($\rho_{0.88\mu m}$) and $\rho_{0.88\mu m}$ can be used to identify its presence. Hall et al. (1998) defines the NDSI as

$$NDSI = \frac{\rho_{0.55\mu m} - \rho_{1.62\mu m}}{\rho_{0.55\mu m} + \rho_{1.62\mu m}}. \quad (2\text{-}2)$$

When sea ice is present, $T_B(11\mu m)$ will be below 280°K and the NDSI will be computed. If the NDSI > 0.4 and $\rho_{0.88\mu m} > 0.1$ then sea ice is possibly present.

Finally, a test is needed to ensure that the assumed sea ice is not a high, cold cloud. Two bands are included in the Hall Test that are sensitive to high clouds. The atmosphere has a low tranmittance at 13μm due to CO_2 absorption and at 1.38μm due to water vapor absorption. In both cases, radiance from the lower troposphere is removed by absorption and only radiance emitted or reflected from the upper troposphere contributes to the radiance measured by the sensor. If $T_B(13\mu m) < 220°K$ and $\rho_{1.38\mu m} > 0.035$, the Hall test assumes that high cloud is present in the pixel and is responsible for the false-positive assignment of sea ice.

When applying the Hall Test, it is important to remember that polar ocean water has a very low albedo compared to that of the highly reflective arctic sea ice. Complications arise when dealing with "New Ice" (Frazil, Grease, Slush or Shuga) that has a thickness between 0 and 10 cm. There might not be enough contrast in reflectance ($\rho_{0.88\mu m}$) to adequately separate the sea ice from water. In addition, as sea ice melts, water will pool on top of the floe and lower the albedo so the pixel will appear to be water when, in fact, it is sea ice.

For the operational MODIS cloud mask, sea ice is present only when either the NCEP or the NSIDC sea ice product and when the Hall Test detects the of sea ice. MAS only uses the Hall Test to detect the presence of sea ice.

3. Groups and Test

The five groups within the cloud mask are comprised of various tests. The number of groups and tests are determined by the input values. The groups that are important to the ocean polar regions are described below.

a. Group 1

The objective of Group 1 is to identify thick high clouds based on infrared T_B characteristics. This is accomplished in the ocean polar regions with $T_B(11\mu m)$ and $T_B(13.9\mu m)$ wavelengths tests. The group has a potential difficulty with low clouds that have small thermal contrast between the cloud and the surface (Ackerman et al., 1997).

(1) $T_B(11\mu m)$ Test. This is a simple IR cloud test that can obtain information about the surface or cloud top temperature. It is also important when dealing with the detection of snow covered sea ice as described above. In the open ocean when $T_B(11\mu m)$ channel is expected to be less than 270°K ,the mask assumes the pixel is too cold to be open ocean and determines that it has failed the clear sky condition. In the polar ocean regions, where there might be subpixel sea ice present, there is a need to lower the $T_B(11\mu m)$ threshold values. The magnitude of this modification will be discussed in the next chapter. In general, simple thresholds should vary with location, season, and time of day.

(2) $T_B(13\mu m)$ Test. This test relies on the absorption characteristics of CO_2. Clouds being sensed by a CO_2 band depend upon the atmospheric

attenuation in that band and the altitude of the cloud. The spectral band at 13.9μm provides good sensitivity to the relatively cold regions of the atmosphere. Only clouds above 500 hPa will have strong contributions to the radiance at the top of the atmosphere observed at 13.9μm. Lower regions of the atmosphere and the earth's surface should provide negligible contributions to the radiance at 13.9 μm wavelength (Ackerman et al., 1997).

b. Group 2

The objective of Group 2 is to detect thin clouds missed by Group 1 using infrared T_B differences. T_B difference techniques using MODIS will be very sensitive to thin clouds if the surface emittance and temperature are adequately characterized. Given a surface at 300°K and a cloud at 220°K, a cloud emittance of 0.01 increases the infrared window T_B by 0.5°K. Since the anticipated noise equivalent temperature for many MODIS infrared window spectral bands is better than 0.05°K, the cloud mask should be very sensitive to thin cloud (Ackerman et al., 1997).

(1) Tri-Spectral Technique. Ackerman et al. (1997), suggests the use of a tri-spectral technique with $T_B(8\mu m)$ - $T_B(11\mu m)$ and $T_B(11\mu m)$ - $T_B(12\mu m)$ tests for thin cirrus clouds when precipitable water (pw) is greater than 1.0cm. A polar atmosphere is relatively dry and pw is less than 1.0cm. Therefore, only the $T_B(11\mu m)$ - $T_B(12\mu m)$ test is used to detect thin cirrus clouds. As will be discussed in the next chapter, MAS data suggests that this test might not be viable in daytime polar ocean regions.

(2) $T_B(3.9\mu m)$ - $T_B(11\mu m)$. This test is used to identify fog and low clouds. Clouds at 11μm wavelength, independent of water droplet size, are very close to being black bodies, with emittance approximatley equal to 1. Clouds at 3.9μm wavelength are not black bodies and emittance is a function of water droplet size. For a normal water droplet size of 10μm, the emittance is approximately 0.85.

During the day, the $T_B(11\mu m)$ is composed of only energy that has been emmitted from the cloud and is very close to the actual cloud top temperature. The $T_B(3.9\mu m)$ during the day is composed of both energy that is emmitted and reflected from the cloud. This will raise the sensed temperature above the actual cloud top temperature. Therefore, a positive difference in the $T_B(3.9\mu m)$ - $T_B(11\mu m)$ test is an indication of liquid water clouds during the day.

At night, negative values for $T_B(3.9\mu m)$ - $T_B(11\mu m)$ indicate a liquid water cloud. $T_B(3.9\mu m)$ is only a function of emmitted energy and will be less than the actual temperature since the emittance is less than one. Therefore, small $T_B(3.9\mu m)$ - $T_B(11\mu m)$ differences are observed when clouds are optically thick due to reduced emmitance at $T_B(3.9\mu m)$.

c. Group 3

The objective of Group 3 is to detect low clouds by using solar reflectance and reflectance ratio tests and is especially sensitive to thick, low clouds. It complements Group 1 because it is sensitive to thick, low level clouds while Group 1 has difficulty with low clouds that have small thermal contrast between cloud and background. This

technique works well when there is a high contrast in the reflectance between the surface and the cloud, for example, clouds over water.

(1) $\rho_{0.88\mu m}$. This is a single band threshold test that does well for discriminating bright clouds over dark surfaces (e.g., stratus over ocean) and poorly for clouds over bright surfaces (e.g., sea ice). The reflectance test is adjusted for viewing angle and the test is eliminated when a sun glint condition exists for the pixel (Ackerman et al., 1997).

(2) Ratio of $\rho_{0.87\mu m}/\rho_{0.66\mu m}$. Many earth surface features are less reflective at visible wavelengths than they are at near-IR wavelengths. Clouds do not exhibit these same variations in reflectance to any great degree (Ackerman et al., 1997).

d. Group 4

The objective of Group 4 is to detect high thin cirrus clouds during the day. Due to the fact that most of the atmosphere's water vapor is located in the low to mid troposphere, most of the reflectance from the surface, low, and mid level clouds, should be attenuated prior to reaching any space borne sensor when sufficient water vapor (0.4 cm precipitable water) is in the atmosphere. Gao et al. (1993) developed a technique to detect the presence of thin cirrus clouds by a strong water vapor absorption band in the near-IR at 1.38μm (MAS - 1.88μm) wavelength. This band receives large amounts of scattered solar radiance when thin cirrus clouds are present. Ackerman et al. (1997) placed this technique in to its own group because they felt "there was no test that has been found to be as sensitive to the presence of thin cirrus."

e. Group 5

The objective of Group 5 is similar to those of Group 2 in that it is designed to detect thin clouds. However, in this case the focus is on thin cirrus clouds at night. In the polar ocean regions, a $T_B(3.9\mu m)$ - $T_B(11\mu m)$ difference is employed to detect cirrus clouds and is relatively insensitive to the amount of water vapor in the atmosphere (Hutchison and Hardy, 1995). This test is greater than zero in semitransparent cirrus as sub-pixel warm features dominate the shortwave window radiances within a pixel.

THIS PAGE INTENTIONALLY LEFT BLANK

III. MAS/MODIS CLOUD MASK

MAS offers the opportunity to test the validity of the cloud mask prior to the MODIS launch. Subjective analysis of the cloud properties are compared with cloud mask results. Modifications of tests and thresholds are then suggested to improve the cloud mask performance.

A. OPTIMIZING THE CLOUD MASK

MAS Flight #97-73 is a daytime flight from the FIRST ISSCP Regional Experiment - Arctic Cloud Experiment (FIRE/ACE) flight of June 2 - 3, 1998 and is used as a case for cloud mask optimization in the polar ocean region. Figure 3.1 shows the over-ground track of the ER-2 aircraft.

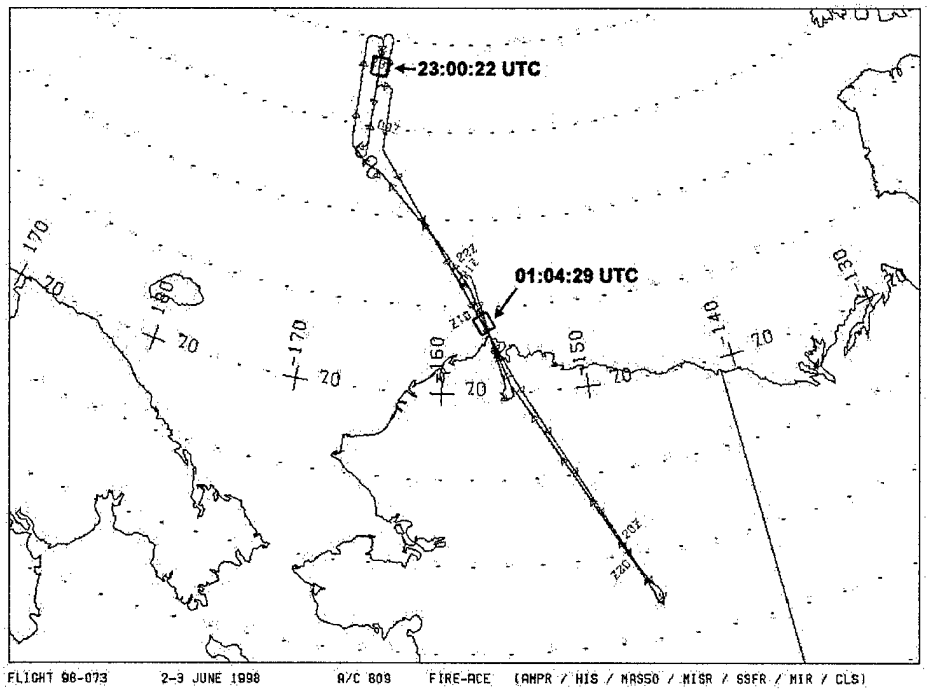

Figure 3.1. The ER-2 over-ground track is plotted for MAS Flight #98-73, June 2 - 3, 1998. (Gumley et al., 2000) The two regions of the flight used for cloud mask optimization are identified as blue squares.

1. Original Cloud Mask

Figure 3.2 is an annotated RGB image (Red: Band 20, Green: Band 10, Blue: Band 2) of track 17, center time of 01:04:29 UTC with Pt Barrow to the top of the image (South). The scene contains an area of mid to low clouds over a pack of mixed multi-year and first-year sea ice that dominates most of the scene. The Marginal Ice Zone (MIZ) is the transition area between pack ice and lesser concentrations of ice. Take note of the belting of sea ice jetting into water from the main pack ice. An area of 40 - 60% concentration of multi-year and first-year sea ice is located in the upper left hand corner of the scene.

The original cloud mask classifies the scene as one of two types, *Ocean Polar Snow Day* or *Ocean Day*. This classification is very dependent on the Hall Test described in Chapter II. Table 3.1 lists the original group, test and thresholds for the two scene types.

Table 3.1. Original Groups, Tests, and Thresholds

Polar Ocean Snow Day			***Ocean Day***		
Group	**Test**	**Threshold (α, β, γ)**	**Group**	**Test**	**Threshold (α, β, γ)**
1	$T_B(13.9\mu m)$	219,220,221	1	$T_B(11\mu m)$	267, 270, 273
				$T_B(13.9\mu m)$	219,220,221
2	$T_B(3.9\mu m) - T_B(11\mu m)$	11.0, 9.0, 7.0	2	$T_B(11\mu m) - T_B(12\mu m)$	Dynamic
				$T_B(11\mu m) - T_B(3.9\mu m)$	-10, -8, -6
			3	$\rho_{0.88\mu m}$	8, 7, 6.5
				$\rho_{0.87\mu m}/\rho_{0.66\mu m}$	0.95, 1.10, 1.15 0.95, 0.90, 0.85
4	$\rho_{1.38\mu m}$ (MAS - $\rho_{1.88\mu m}$)	4.0, 3.5, 3.0	4	$\rho_{1.38\mu m}$ (MAS - $\rho_{1.88\mu m}$)	4.0, 3.5, 3.0

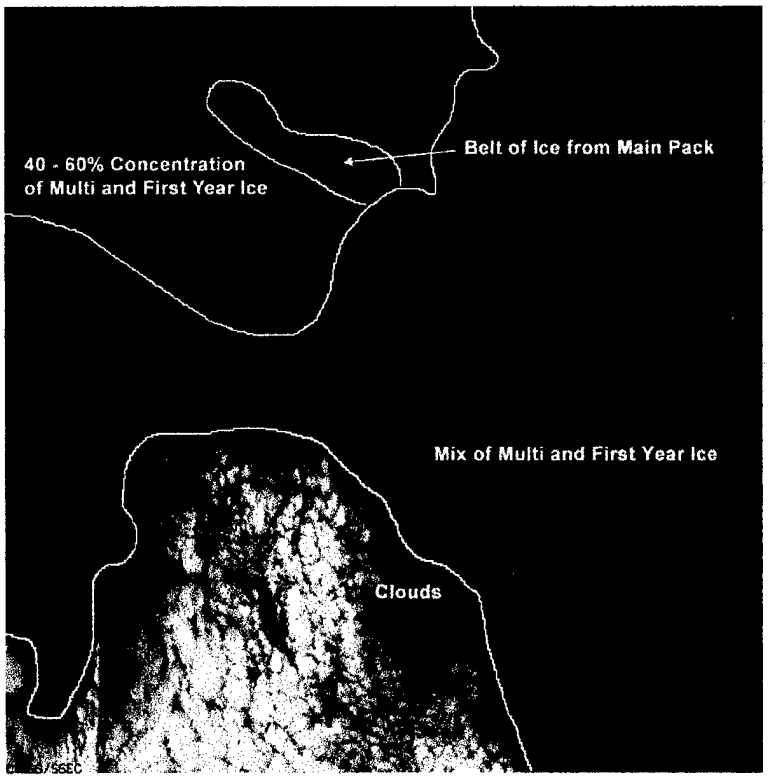

Figure 3.2. MAS Flight #97-73, Track 17, Center Time of 01:04:29 UTC is displayed as an RGB image where Red is band 20, Green is band 10, Blue is band 2. Clouds, multi-year and first-year sea ice and partial ice concentration area are noted.

Figure 3.3 shows the original cloud mask correctly classifying most of the clouds as *Cloudy*. It also correctly classifies the clear region over the pack ice as *Confident Clear*. The cloud mask encounters difficulty along the MIZ, where it classifies the clear areas as either *Undecided* or *Cloudy*. It also has trouble in the water areas where the pixel is clear of clouds and sea ice, but the mask still classifies it as either *Probably Clear*, *Undecided* or *Cloudy*.

a. Hall Test

The Hall Test is very important in determining which scene type is used in the cloud mask. Since the entire scene is below 280°K for $T_B(11\mu m)$, the Hall Test is

initiated everywhere in the scene. Figure 3.4 shows the NDSI and $\rho_{0.88\mu m}$ tests for this scene. With the exception of a few cloudy pixels, the NDSI test classifies most of the scene as possibly being sea ice. The $\rho_{0.88\mu m}$ test checks the scene reflectance and classifies the polar water area as free of sea ice if the reflectance is less than 0.10 (green areas in Figure 3.4).

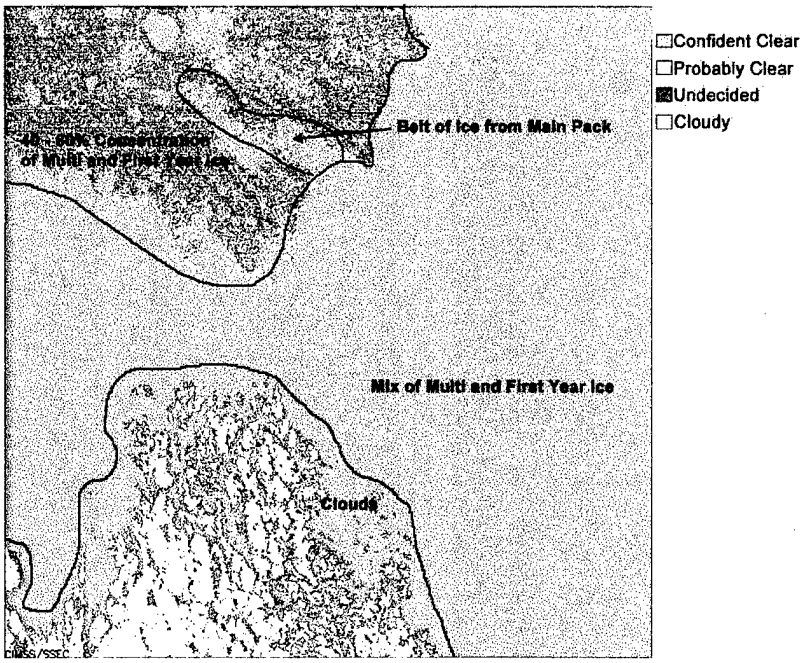

Figure 3.3. Original Cloud Mask is applied to MAS Flight #97-73, Track 17, Center Time of 01:04:29 UTC. Mask classifications are described in the legend.

Figure 3.5 shows that the Hall Test correctly identifies the pack ice and much of the cloudy region. The test identifies some of the clouds as sea ice but as will be seen latter, are eventually classified as *Cloudy* when the final confidence value is computed. Finally, the floating sea ice in the partial ice concentration area is correctly

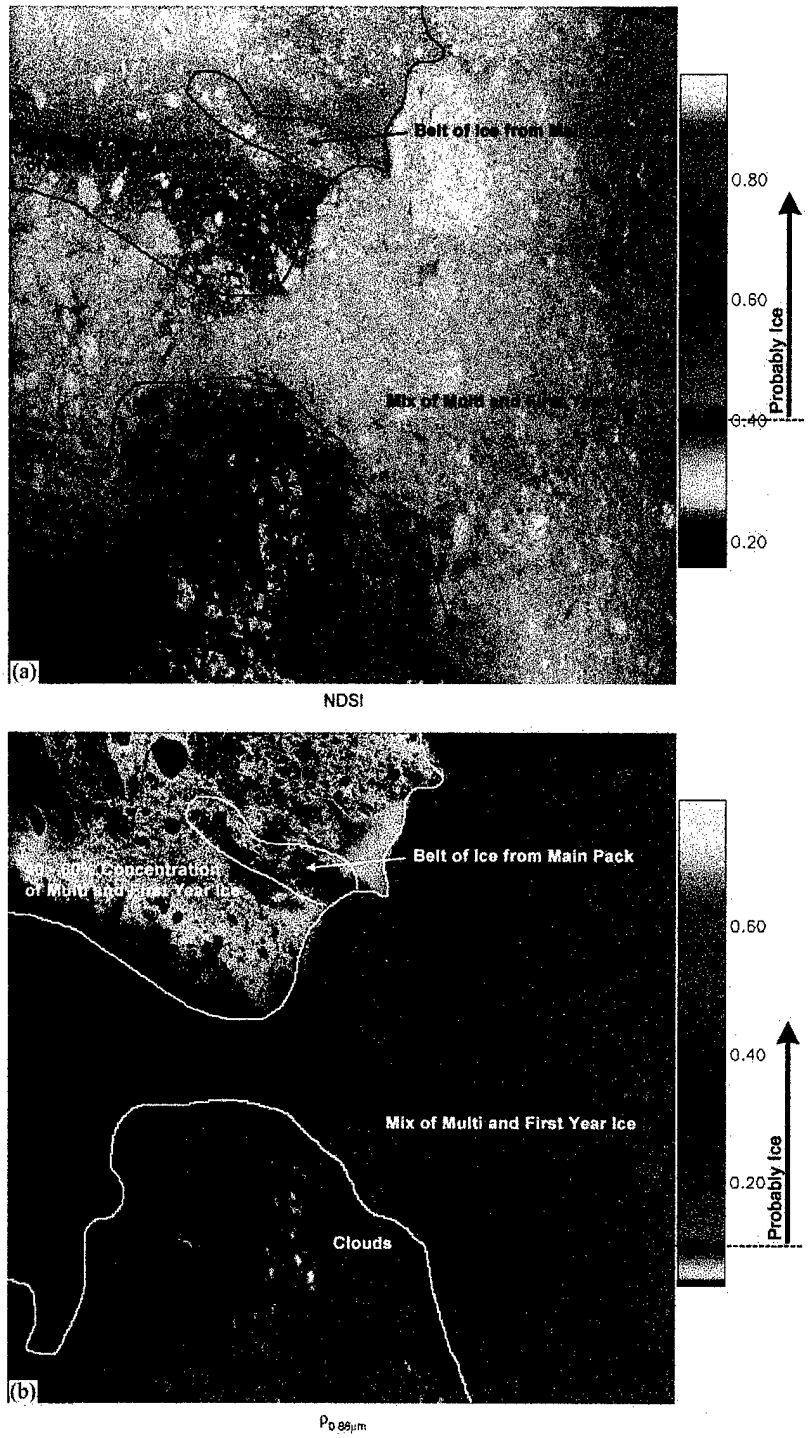

Figure 3.4. The NDSI test (a) and the $\rho_{0.88\mu m}$ test (b) is applied to MAS Flight #97-73, Track 17, Center Time of 01:04:29 UTC. The figures are colored according to the thresholds set for each test. The NDSI test classifies pixels with values greater than 0.4 as *Probably Ice*. The $\rho_{0.88\mu m}$ classifies pixels with values greater than 0.1 as *Probably Ice.*

identified as sea ice. Therefore, the Hall Test properly classifies pixels and initiates the groups and tests that need to be conducted for cloud detection.

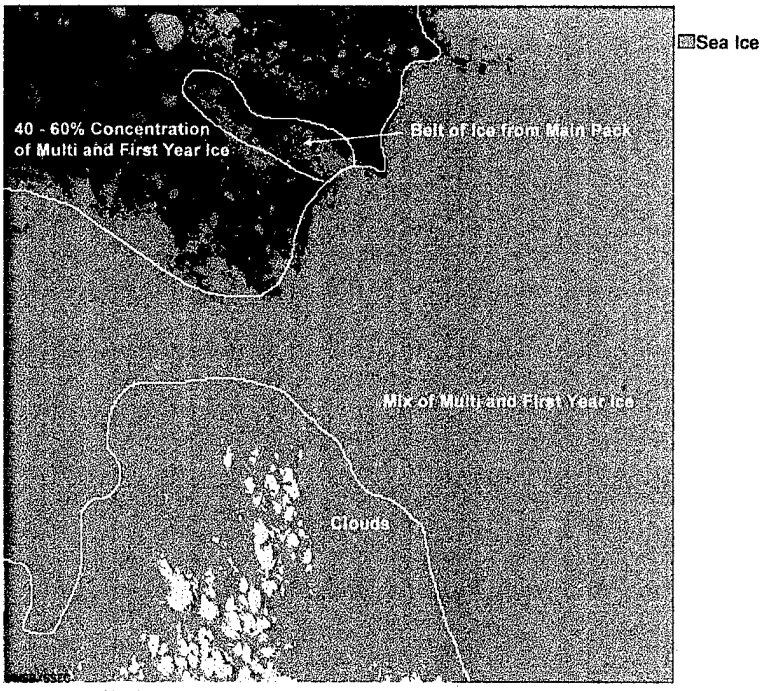

Figure 3.5. MAS Flight #97-73, Track 17, Center Time of 01:04:29 UTC, Hall Test. Mask classifications are described in the legend.

b. Individual Pixels

Figure 3.3 reveals the greatest misidentification in this scene that occurred along the MIZ and the partial ice concentration area. Two representative pixels are selected to investigate this error. They are 1 and 2 pixels away, respectfully, from the main pack ice. Table 3.2 lists test results for a pixel that is classified as sea ice by the Hall Test and uses the groups and tests that correspond with *Polar Ocean Snow Day*. Table 3.3 lists test results for a pixel that is immediately adjacent to the first pixel and is classified as water and therefore uses the groups and tests that correspond with *Ocean Day*.

Table 3.2. *Polar Ocean Snow Day* Pixel Values for MAS Flight #97-73, Track 17, Center Time of 01:04:29 UTC, Scanline124304, Sample 305

Scanline	124304	**Sample**	305	
Group	**Test**	**Threshold (α, β, γ)**	**Value**	**Confidence**
1	$T_B(13.9\mu m)$	219,220,221	254.87	1
2	$T_B(3.9\mu m) - T_B(11\mu m)$	11.0, 9.0, 7.0	-2.72	1
4	$\rho_{1.88\mu m}$	4.0, 3.5, 3.0	0.52	1
		Overall Confidence (Q)		1

Table 3.3. *Ocean Day* Pixel Values for MAS Flight #97-73, Track 17, Center Time of 01:04:29 UTC, Scanline124304, Sample 306

Scanline	124304	**Sample**	306		
Group	**Test**	**Threshold (α, β, γ)**	**Value**	**Test Confidence**	**Group Confidence**
1	$T_B(11\mu m)$	267, 270, 273	270.76	0.63	0.63
	$T_B(13.9\mu m)$	219,220,221	255.13	1	
2	$T_B(11\mu m) - T_B(12\mu m)$	1.136656, 0.636656, -0.61334	-0.05	0.77	0.77
	$T_B(3.9\mu m) - T_B(11\mu m)$	-10, -8, -6	2.29	1	
3	$\rho_{0.88\mu m}$	8, 7, 6.5	7.93	0.03	0.03
	$\rho_{0.87\mu m}/\rho_{0.66\mu m}$	0.95, 1.10, 1.15 0.95, 0.90, 0.85	0.83	1	
4	$\rho_{1.88\mu m}$	4.0, 3.5, 3.0	0.40	1	1
				Overall Confidence (Q)	0.36

When the cloud mask classifies the pixel as sea ice (Table 3.2), an overall confidence value of 1 is generated for the pixel. Even though the wrong scene type was initially selected, the cloud mask properly identifies the pixel as *Confident Clear*. When the cloud mask classifies the pixel as water (Table 3.3), the overall confidence value of 0.36 is generated for the pixel. The correct scene type is selected but the cloud mask incorrectly identifies the pixel as *Cloudy*. The confidence values range from *Possibly Clear* to *Cloudy* when the surface is water and the confidence value is *Confident Clear* when the surface is sea ice.

The Hall Test may identify the pixel as water when a pixel possesses sub-pixel sea ice. The $\rho_{0.88\mu m}$ test threshold for the *Ocean Day* scene type is sensitive enough to detect the increased reflectance from the pixel due to subpixel sea ice. If the reflectance is too great for water, the clear confidence level from the $\rho_{0.88\mu m}$ test decreases. This occurs in the MIZ where sub-pixel sea ice occurrence is high. $T_B(11\mu m)$ and $T_B(11\mu m)$ - $T_B(12\mu m)$ tests also have low clear confidence levels (0.63 and 0.77 respectfully) but are not as dependent on the presence of sub-pixel sea ice and are therefore better candidates for the threshold adjustments necessary for optimized cloud detection in polar ocean regions.

c. $T_B(11\mu m)$

The $T_B(11\mu m)$ test produced a 0.63 clear confidence level that the pixel was clear for the *Ocean Day* scene type case. Figure 3.6(a) shows the RGB image of the scene with the $T_B(11\mu m)$ test result overlaid where the test was conducted. The clouds are not cold enough to be classified as *Cloudy* according to the original threshold, while the partial ice concentration area is not warm enough to be classified as *Confident Clear.*

Surface temperature controls the value of $T_B(11\mu m)$ when corrected for surface emittance and given low water vapor content. Hall et al. (1998) used data from MAS images collected in April 1995, near St. Lawrence Island, Alaska, and estimated the mean seawater temperature to be 271.6°K using seawater emittance of 0.985. Based on direct measurement, the freezing point of polar ocean water was found to be 271.4°K. Therefore, any pixel can be classified as possibly sea ice if its surface temperature is less than or equal to 271.4°K, the freezing point of polar seawater.

Figure 3.6(b) is similar to 3.6(a) except the NPS modified threshold for $T_B(11\mu m)$ test is applied. The threshold was lowered by 1°K from the original threshold. Polar ocean water is now warm enough to be identified as clear (white), while clouds are still cold enough to be identified as clouds since they are colder that the β–threshold (β = 272°K).

When the NPS threshold is applied to the $T_B(11\mu m)$ test and the cloud mask is run, the clear confidence level of the test pixel was increased to 0.79 from the previous value of 0.63. Figure 3.7 shows the original cloud mask (a) compared with the cloud mask with the modified NPS $T_B(11\mu m)$ threshold (b). The clear confidence level increases for many of the pixels in the partial ice concentration area. The clouds are still identified as *Cloudy*. However, an unacceptable number of pixels are still classified as *Undecided.*

d. $T_B(11\mu m) - T_B(12\mu m)$

Figure 3.8 shows the $T_B(11\mu m) - T_B(12\mu m)$ test colorized for an average view angle and $T_B(11\mu m)$ threshold. It is difficult to obtain any information about the scene from this test. Therefore, this test is removed from the *Ocean Day* scene type tests in the optimized cloud mask.

Figure 3.9 shows the original cloud mask (a) compared with the cloud mask without the $T_B(11\mu m) - T_B(12\mu m)$ test. There is significant improvement of the cloud mask in the partial ice concentration area showing fewer pixels as *Cloudy* or *Undecided.* Most of the water region has changed to *Probably Clear* with much of the noise is removed

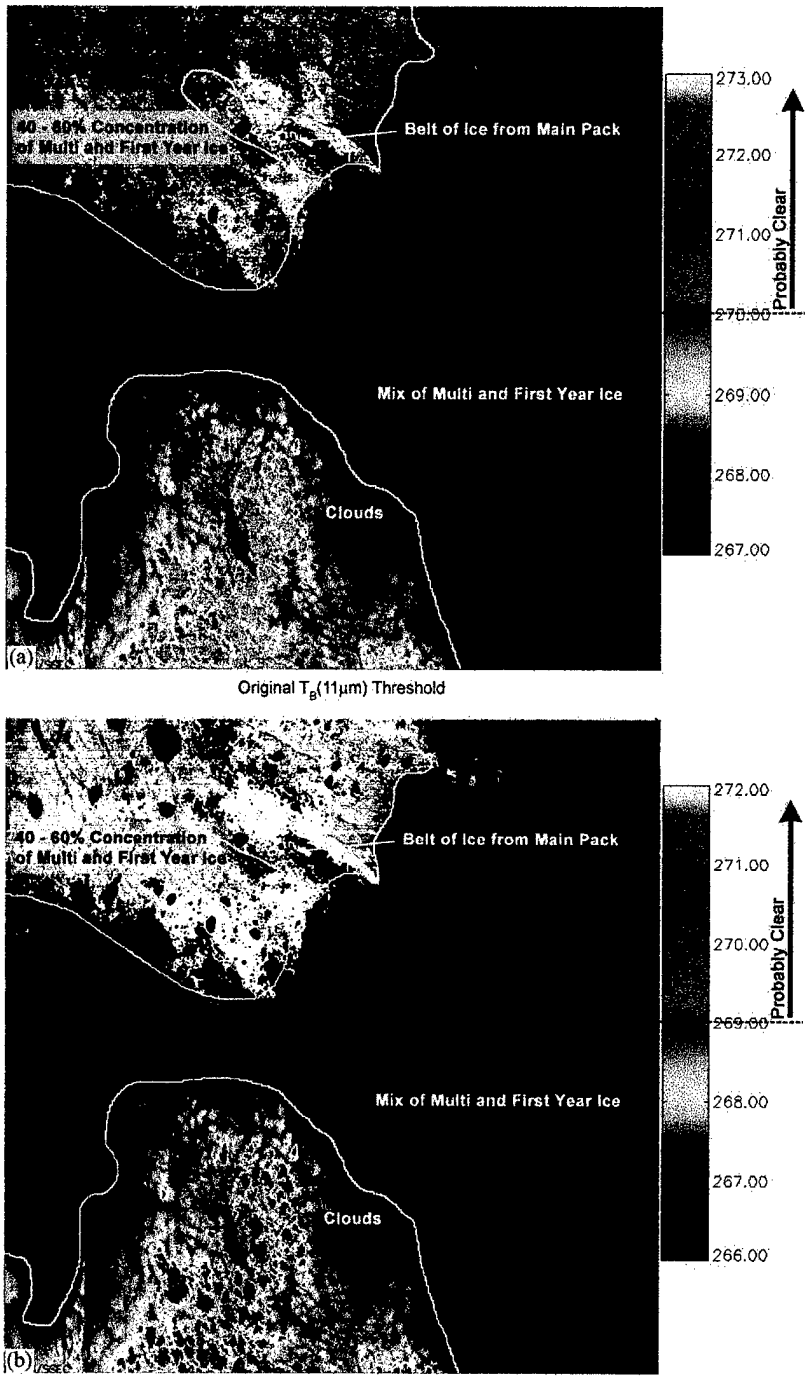

Figure 3.6. Original T_B(11μm) test threshold (a) and the NPS T_B(11μm) test threshold (b) are applied to MAS Flight #97-73, Track 17, Center Time of 01:04:29 UTC and overlaid on a RGB images. The figures are colored according to the thresholds set for each test. The original threshold classifies values greater than 270°K as *Probably Clear*. The NPS threshold classifies values greater than 269°K as *Probably Clear*.

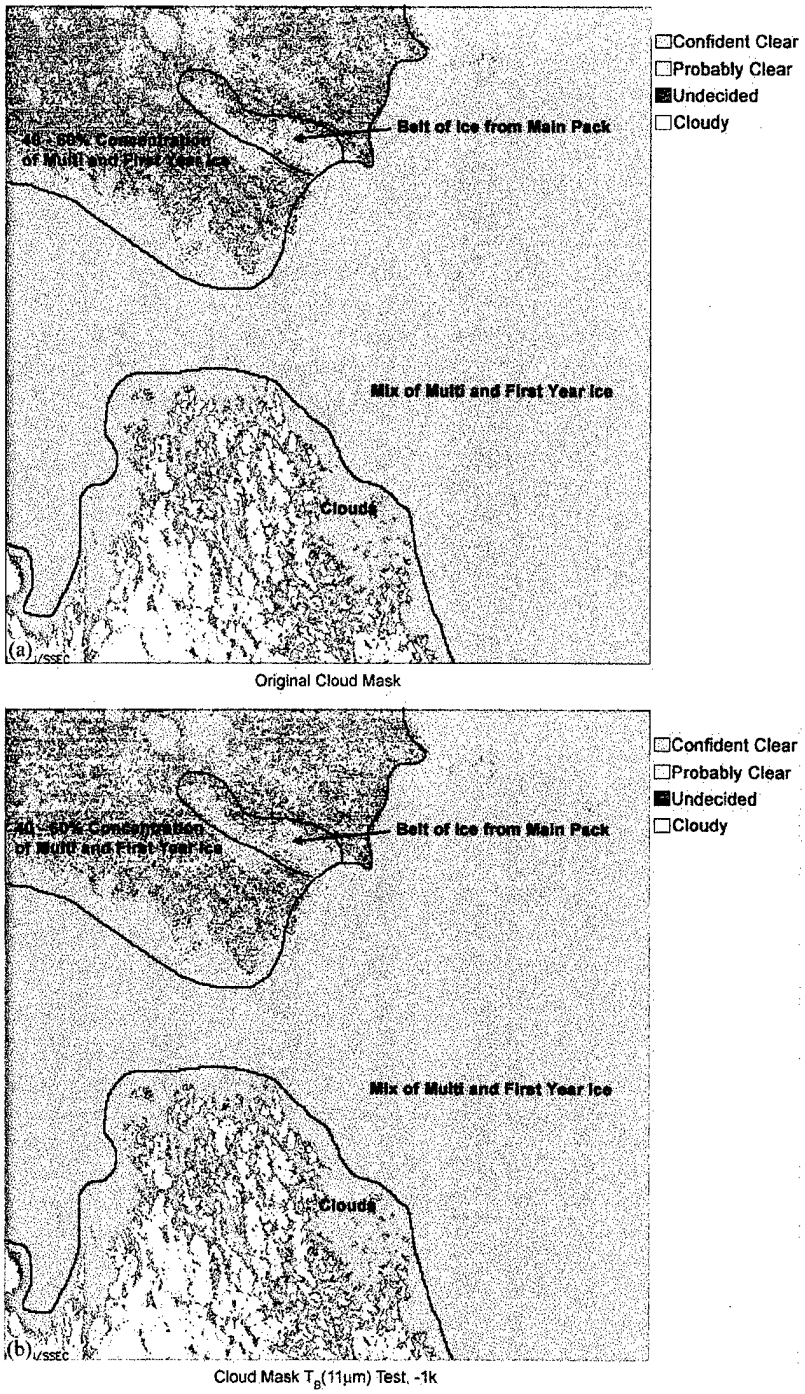

Figure 3.7. Original cloud mask (a) and the NPS cloud mask (b) are applied to MAS Flight #97-73, Track 17, Center Time of 01:04:29 MAS Flight #97-73, Track 17, Center Time of 01:04:29 UTC. Mask classifications are described in the legend.

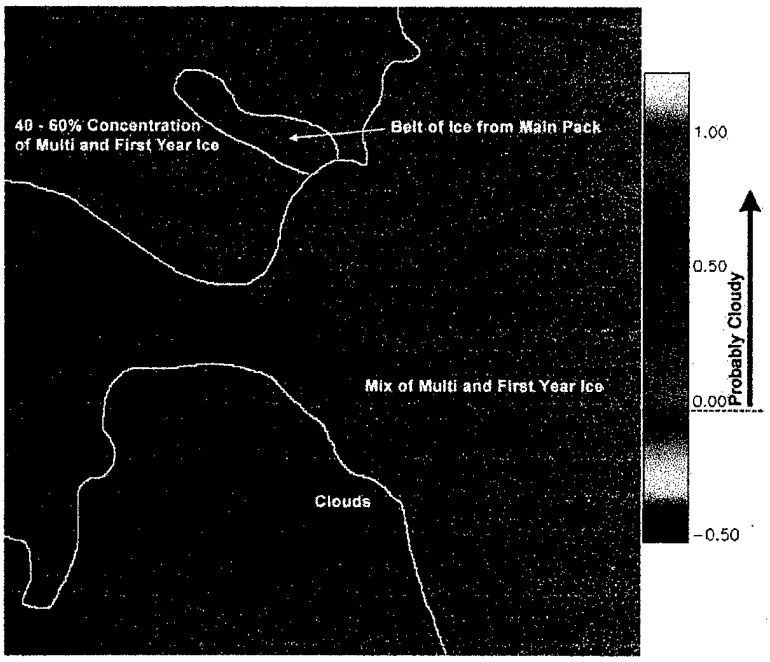

Figure 3.8. The $T_B(11\mu m)$ - $T_B(12\mu m)$ test is applied to MAS Flight #97-73, Track 17, Center Time of 01:04:29 UTC. The scene is colorized for an average threshold.

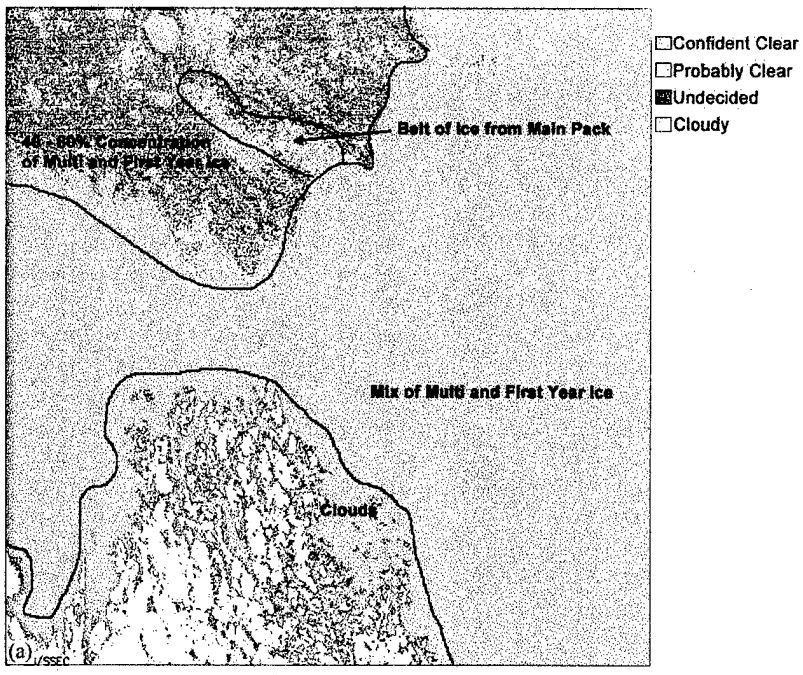

Original Cloud Mask

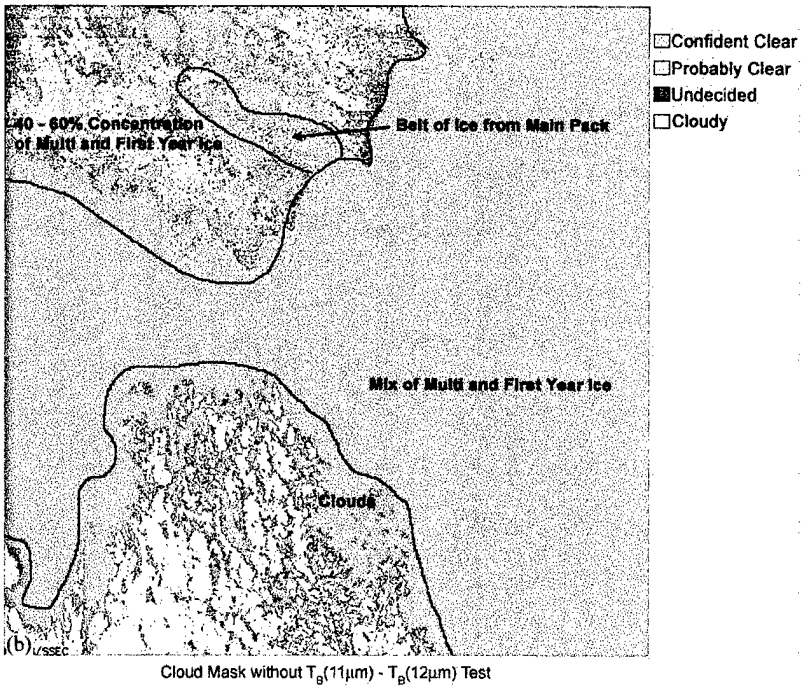

Cloud Mask without $T_B(11\mu m) - T_B(12\mu m)$ Test

Figure 3.9. Original cloud mask (a) and the NPS cloud mask (b) are applied to MAS Flight #97-73, Track 17, Center Time of 01:04:29 MAS Flight #97-73, Track 17, Center Time of 01:04:29 UTC. Mask classifications are described in the legend.

e. $T_B(3.9\mu m) - T_B(11\mu m)$

Once the new threshold was defined for $T_B(11\mu m)$ and the $T_B(11\mu m)$ - $T_B(12\mu m)$ test was removed, other scenes indicated the $T_B(3.9\mu m)$ - $T_B(11\mu m)$ test threshold might not be sensitive enough to detect low clouds. To be consistent throughout the algorithm, the $T_B(11\mu m)$ - $T_B(3.9\mu m)$ test in the *Ocean Day* scene type was changed to $T_B(3.9\mu m)$ - $T_B(11\mu m)$. The only difference in the test is a sign change.

Figure 3.10 shows Track 9 of FIRE/ACE Flight #97-73, with a center time of 23:00:22 UTC and is an example where the entire scene is classified as sea ice on the surface and is dominated by thick low to mid-level clouds above. Dark shadows and semi-transparent clouds near the top of the scene might affect the performance of the cloud mask. Finally, along the bottom, multi-year sea ice is visible through the thin, broken low-level clouds.

Figure 3.11 shows the original cloud mask. The original cloud mask over-characterized the scene as *Confident Clear*, especially in the dark shadow and semi-transparent area where high clouds are casting a shadow over low clouds. The original cloud mask also had difficulty detecting the thin, broken, low-level clouds.

The cloud mask modified with the new $T_B(11\mu m)$ threshold and with $T_B(11\mu m)$ - $T_B(12\mu m)$ removed was run but there were no changes in the detection of clouds. This is due to the fact that the entire scene was classified as sea ice and only used *Polar Snow Day* as the scene type. The $\rho_{1.88}$ and $T_B(13.9\mu m)$ thresholds correctly determined the scene contained no high clouds. The $T_B(3.9\mu m)$ - $T_B(11\mu m)$ test is

therefore the only candidate for threshold modification in order to correctly classify the low and mid-level clouds apparent in Figure 3.10.

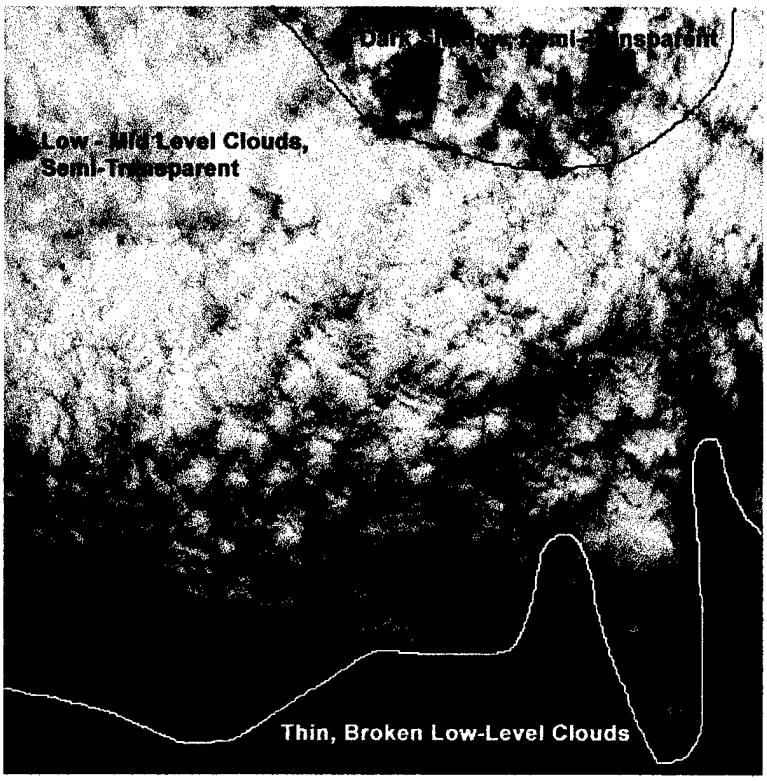

Figure 3.10. MAS FIRE/ACE Flight #97-73, Track 9, Center Time 23:00:22 UTC, is displayed as an RGB image where Red is band 20, Green is band 10, Blue is band 2. Thick low to mid-level clouds dominate the scene with dark shadows and semi-transparent clouds near the top. Finally, along the bottom, multi-year sea ice is visible through the thin, broken low-level clouds.

The $T_B(3.9\mu m) - T_B(11\mu m)$ test has a flipped threshold. The test indicates the scene is *Confident Clear* until it reaches the lower threshold value, and the confidence of the pixel being clear decreases as the test reaches the upper threshold value. At this point, there is zero confidence that the pixel is clear.

Figure 3.12(a) shows the original $T_B(3.9\mu m)$ - $T_B(11\mu m)$ test threshold. The original threshold was unable to identify many of the low clouds in the scene. It also failed to identify the clouds in the dark shadow and semi-transparent area.

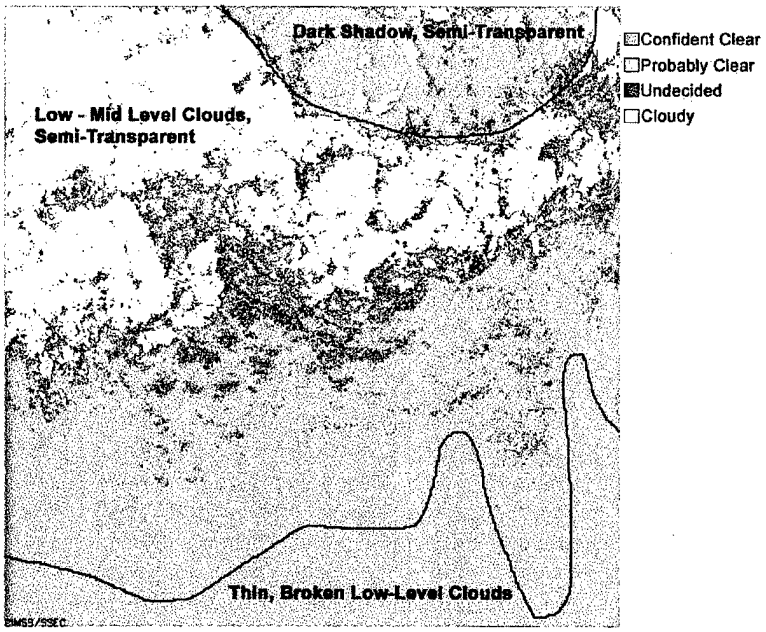

Figure 3-11. Original Cloud Mask is applied to MAS FIRE/ACE Flight #97-73, Track 9, Center Time 23:00:22 UTC. Mask classifications are described in the legend.

Figure 3.12(b) is similar to 3.12(a) except the NPS modified threshold for $T_B(3.9\mu m)$ - $T_B(11\mu m)$ test is applied. The new threshold reduced α from 11 to 5.25, β from 7 to 3.5 and γ from 7 to 1.75. The new threshold improved the detection of the low level clouds in the thin broken and dark shadow, semi-transparent areas. The NPS $T_B(3.9\mu m)$ - $T_B(11\mu m)$ threshold still had trouble where the dark shadows reduced the difference enough to be falsely considered clear.

Figure 3.13 shows the cloud mask with the NPS modified $T_B(3.9\mu m)$ - $T_B(11\mu m)$ test threshold added. The cloud mask detects more low and middle level

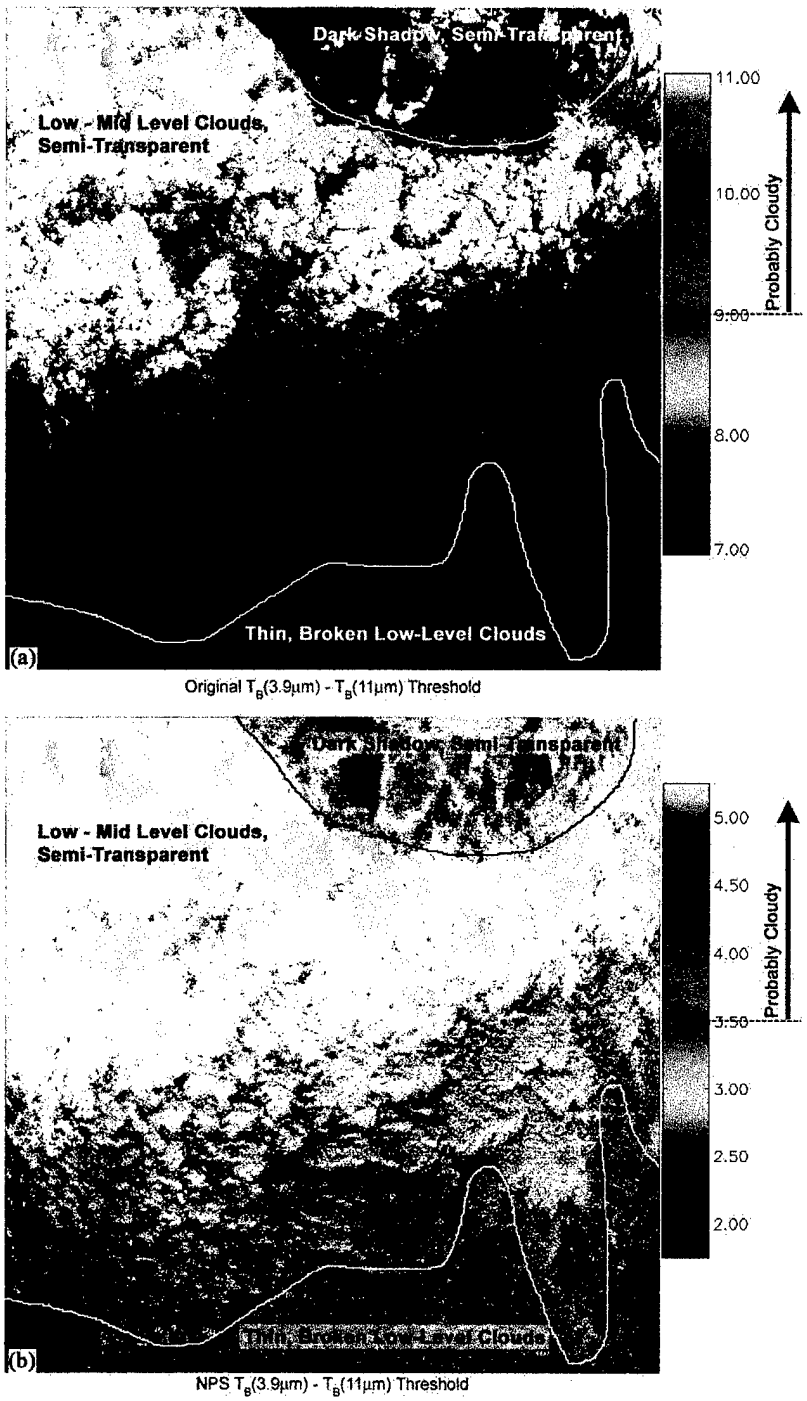

Figure 3.12. Original $T_B(3.9\mu m) - T_B(11\mu m)$ test threshold (a) and the NPS $T_B(3.9\mu m) - T_B(11\mu m)$ test threshold (b) are applied to MAS FIRE/ACE Flight #97-73, Track 9, Center Time 23:00:22 UTC. The figures are colored according to the thresholds set for each test. The original threshold classifies values greater than 9.0 as *Probably Cloudy*. The NPS threshold classifies values greater than 3.5 as *Probably Cloudy*.

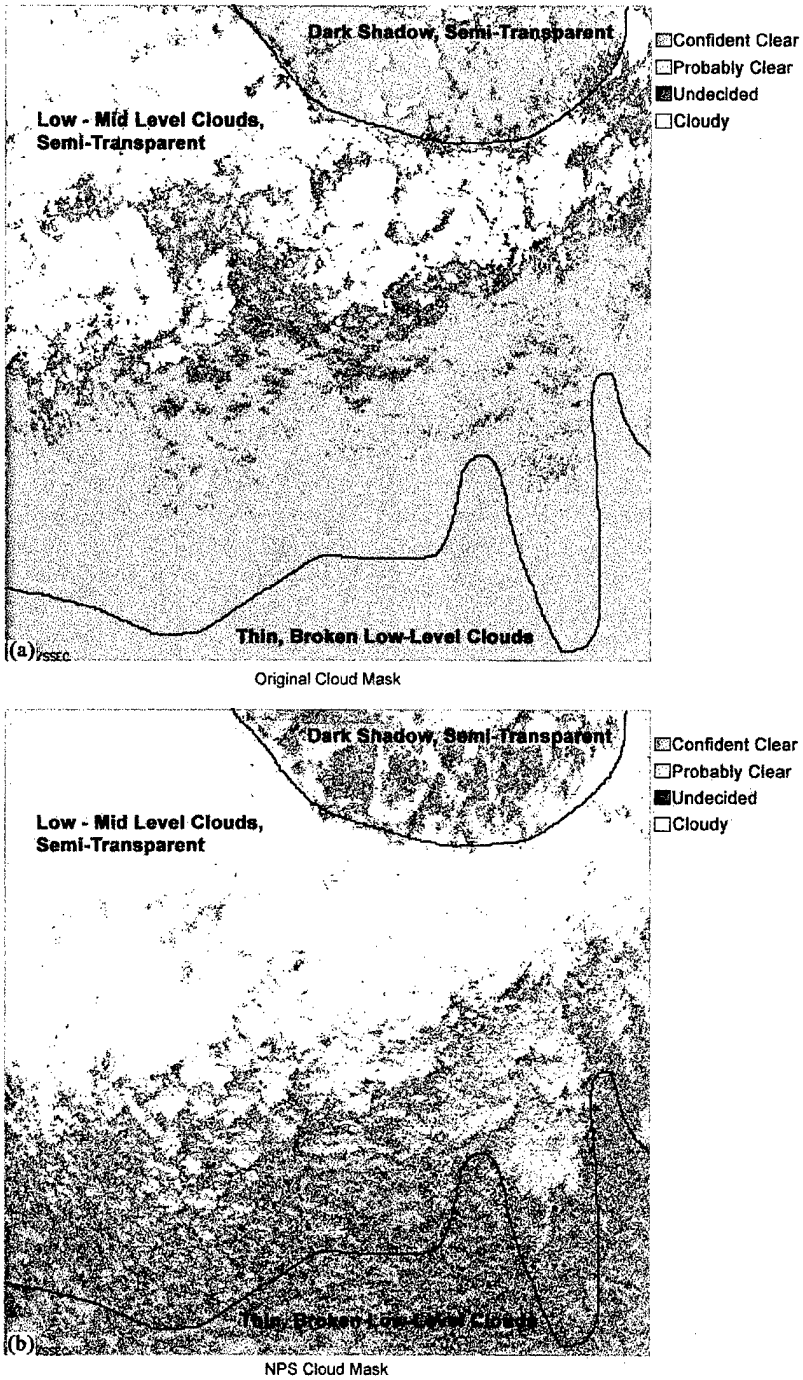

Figure 3.13. Original cloud mask (a) and the NPS cloud mask (b) are applied to MAS Flight #97-73, Track 9, Center Time of 23:00:22 UTC. Mask classifications are described in the legend.

clouds. Only the darkest shadow, semi-transparent area pixels are still classified as *Confident Clear.*

B. NPS MAS/MODIS CLOUD MASK

The observed weaknesses in the original cloud mask were revealed by two new scene type subroutines (*Polar Ice Day* and *Polar Ocean Day).* These scene types were developed after the removal of the $T_B(11\mu m)$ - $T_B(12\mu m)$ test and by identifying the limitations in the thresholds for $T_B(11\mu m)$, and $T_B(3.9\mu m)$ - $T_B(11\mu m)$ tests. These new scene types only run when the pixel is located in a daytime polar ocean region or when sea ice has been detected during the day. Table 3.4 lists the groups, tests and thresholds for these new scene type subroutines.

Table 3.4. New Scene Type Subroutines.

Polar Ice Day			***Polar Ocean Day***		
Group	**Test**	**Threshold (α, β, γ)**	**Group**	**Test**	**Threshold (α, β, γ)**
1	$T_B(13.9\mu m)$	219,220,221	1	$T_B(11\mu m)$	266, 269, 272
				$T_B(13.9\mu m)$	219,220,221
2	$T_B(3.9\mu m) - T_B(11\mu m)$	5.25, 3.5 1.75.	2	$T_B(3.9\mu m) - T_B(11\mu m)$	10, 8, 6
			3	$\rho_{0.88\mu m}$	8, 7, 6.5
				$\rho_{0.87\mu m}/\rho_{0.66\mu m}$	0.95, 1.10, 1.15 0.95, 0.90, 0.85
4	$\rho_{1.38\mu m}$ (MAS - $\rho_{1.88\mu m}$)	4.0, 3.5, 3.0	4	$\rho_{1.38\mu m}$ (MAS - $\rho_{1.88\mu m}$)	4.0, 3.5, 3.0

Figure 3.14 shows the final NPS cloud mask for Track 17, center time of 01:04:29 UTC with the new scene type subroutines. The clouds are better defined and cover a larger area. A few pixels over the cloud-free pack ice are now misclassified as *Undecided* due to the change in the $T_B(3.9\mu m)$ - $T_B(11\mu m)$ test threshold and appears to be related to noisy pixels.

The new scene type subroutines greatly improved the classification of the partial ice concentration area. Most pixels are classified as either *Confident Clear* or *Probably Clear* - a direct result of the $T_B(11\mu m)$ threshold change and the removal of the $T_B(11\mu m) - T_B(12\mu m)$ test.

The NPS cloud mask still has problems with the $\rho_{0.88\mu m}$ test when pixel coverage is *Polar Ocean Day* and sub-pixel sea ice is present. Under these conditions, the reflectance value rises above the threshold, but changing this threshold degrades the ability of the *Polar Ocean Day* scene type to correctly classify the pixel as *Confident Clear* when no sub-pixel sea ice is present. Misclassification is most evident along the MIZ where there is a large concentration of sub-pixel sea ice. The artifact can be used to identify the MIZ or other sea ice edge features. Unfortunately, the problems associated with sub-pixel sea ice contamination will increase as the resolution of the pixel decreases from 50m (for MAS) to 1km (for MODIS). On the other hand, much of the noise in the MAS IR bands will decrease because the comparable MODIS IR bands are expected to have better radiometric sensitivity and more accurate calibration.

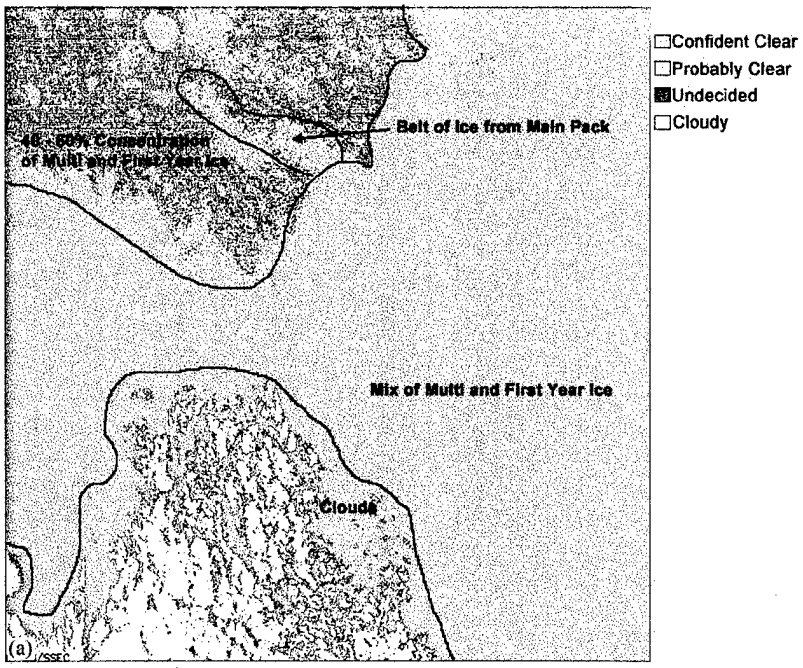

Original Cloud Mask

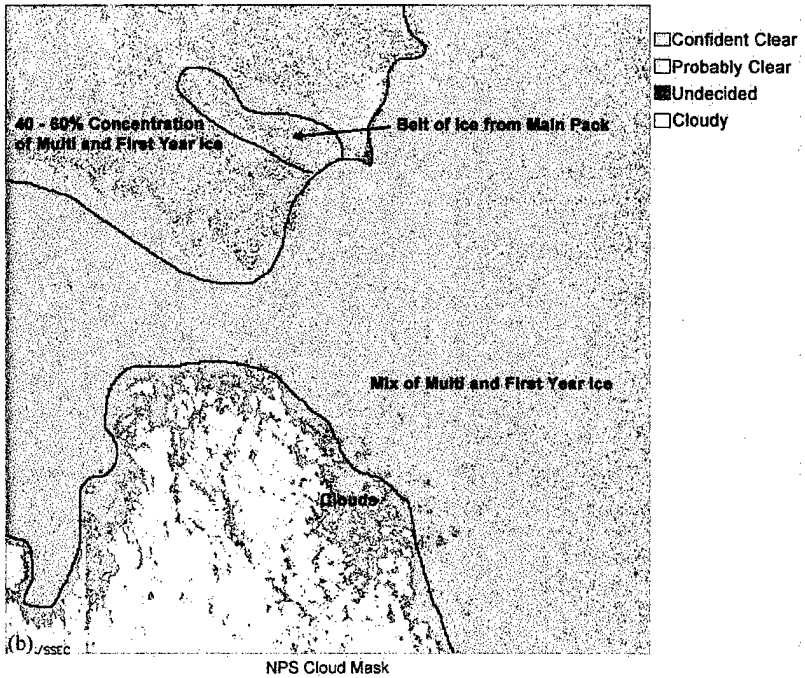

NPS Cloud Mask

Figure 3.14. Original cloud mask (a) and the NPS cloud mask (b) are applied to MAS Flight #97-73, Track 17, Center Time of 01:04:29 UTC. Mask classifications are described in the legend.

THIS PAGE INTENTIONALLY LEFT BLANK

IV. MAS DATA

With the new thresholds in place, other MAS scenes were reviewed to test the optimization of the cloud mask. MAS data from the Winter Cloud Experiment (WINCE), First ISSCP Regional Experiment - Arctic Cloud Experiment (FIRE/ACE) and Winter Experiment (WINTEX) was used to verify the two new scene types. Subjective cloud analysis was done to verify the effectiveness of the new NPS MAS/MODIS cloud mask (NPS cloud mask).

A. MAS FIRE/ACE FLIGHT #98-68, TRACK 6, CENTER TIME 21:04:36 UTC

The MAS FIRE/ACE Flight #98-68 (May 26-27, 1998), track 6, center time 21:04:36 UTC is shown in Figure 4.1.

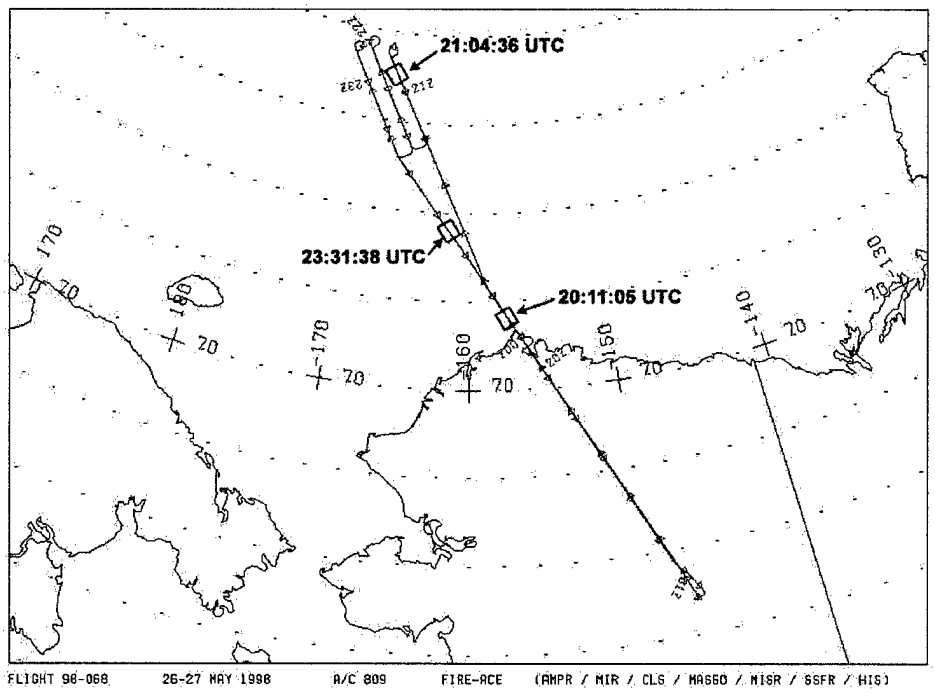

Figure 4.1. MAS FIRE/ACE Flight #98-68, May 26-27, 1998, Flight Track. (Gumley 2000)

This case is an example of a relatively clear arctic condition with a high solar zenith angle (57.9°). Figure 4.2 shows the scene is dominated by sea ice with thin clouds along the right hand side. The Hall Test classified the entire scene as sea ice, therefore only the *Polar Ice Day* scene type was used to detect cloud. The $T_B(13\mu m)$ test detected no high clouds in the scene.

Figure 4.2. MAS FIRE/ACE Flight #98-68, Track 6, Center Time 21:04:36, is displayed as an RGB image where Red is band 20, Green is band 10, Blue is band 2. Sea ice dominated scene with a thin cloud along the right hand side.

Figure 4.3 shows the original cloud mask. It classifies most of the scene as clear with a cloud along the right side of the scene. The striping in the scene is directly related to the noise in the MAS IR bands.

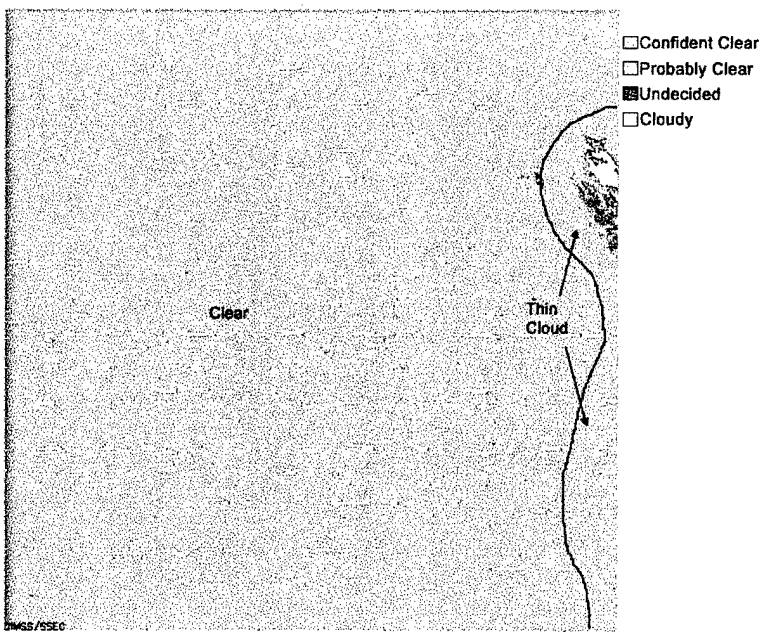

Figure 4.3. Original Cloud Mask is applied to MAS FIRE/ACE Flight #98-68, Track 6, Center Time 21:04:36 UTC. Mask classifications are described in the legend.

Figure 4.4(a) shows the original $T_B(3.9\mu m)$ - $T_B(11\mu m)$ test threshold. The original threshold fails to detect a large portion of the thin cloud. Figure 4.4(b) shows the result of the NPS $T_B(3.9\mu m)$ - $T_B(11\mu m)$ test. The NPS threshold detects much more of the thin cloud and possibly a very thin cloud along the bottom. The NPS threshold results in significantly more noise in the clear area, where it has lowered the final clear confidence value in many of the clear pixels. Again, the lowered values are an artifact of the MAS IR calibration.

Figure 4.5 shows the original and NPS cloud masks. The NPS mask still classifies most of the scene as *Confident Clear*. The NPS threshold results in significantly *Undecided* pixels where it has lowered the final clear confidence value in many of the clear pixels. Identification of these *Undecided* pixels are an important result

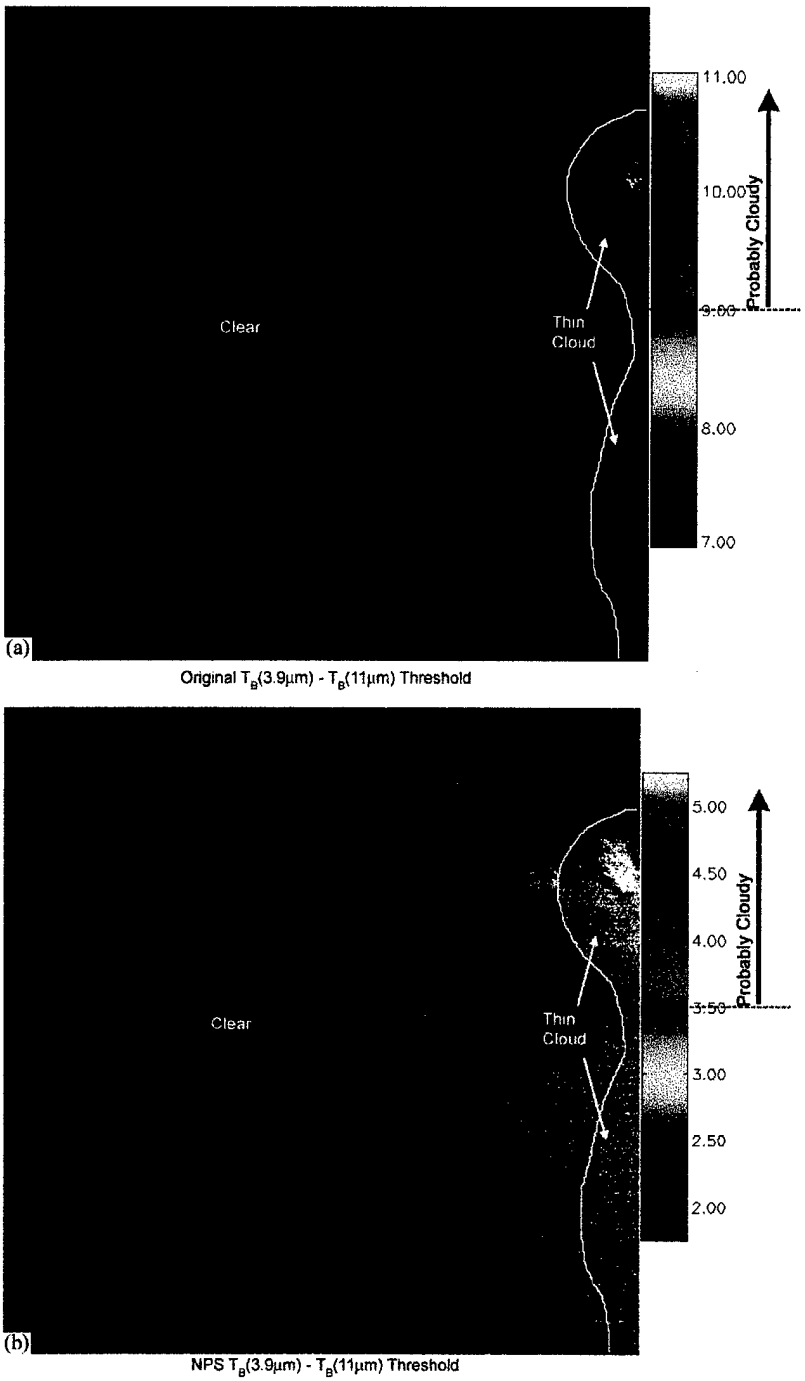

Figure 4.4. Original T_B(3.9μm) - T_B(11μm) test threshold (a) and the NPS T_B(3.9μm) - T_B(11μm) test threshold (b) are applied to MAS FIRE/ACE Flight #98-68, Track 6, Center Time 21:04:36 UTC. The figures are colored according to the thresholds set for each test. The original threshold fails to detect a large portion of the thin cloud. The NPS threshold detects much more of the thin cloud and possibly a very thin cloud along the bottom.

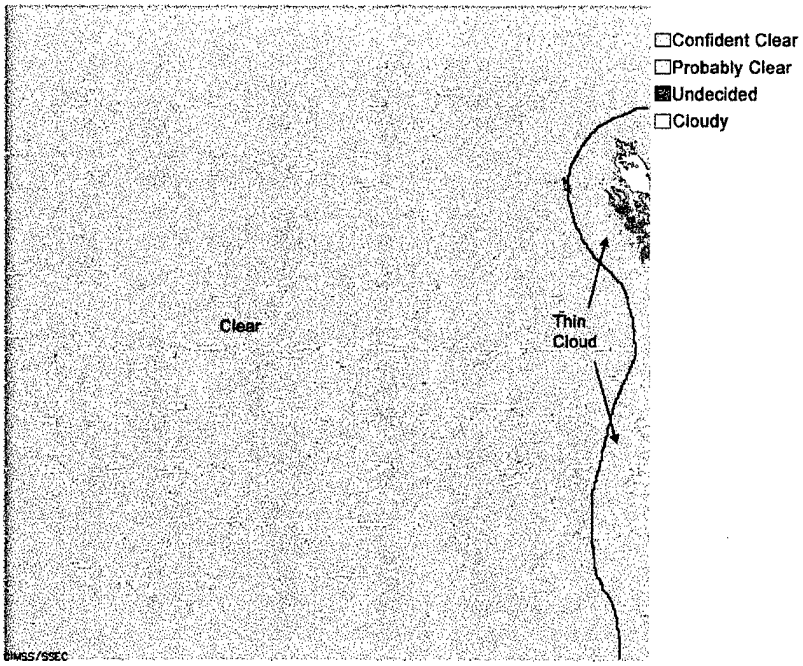

Figure 4.5. Original cloud mask (a) and the NPS cloud mask (b) are applied to MAS FIRE/ACE Flight #98-68, Track 6, Center Time 21:04:36 UTC. Mask classifications are described in the legend. The NPS cloud mask classifies most of the scene as *Confident Clear*, and improves the detection of the thin cloud.

of the variable threshold techniques used in the MAS/MODIS cloud mask. *Undecided* pixels in Figure 4.5 identify regions of very thin clouds that are also apparent in Figure 4.2.

B. MAS FIRE/ACE FLIGHT #98-68, TRACK 16, CENTER TIME 23:31:38 UTC

Figure 4.6 shows the FIRE/ACE Flight 98-68, track 16, center time 23:31:38 UTC. This is an example of a scene that contains both sea ice and high clouds. Clouds are casting a shadow over the sea ice that, at lower spatial resolution, could be misidentified as a lead. As the main cloud thins along its edges, it becomes increasing difficult to distinguish between cloud and sea ice.

Figure 4.7 shows the original cloud mask. It identifies the main cloud mass but has difficulty along the edge. There is no indication of the thin clouds in the center of the scene suggested in Figure 4.6. The Hall Test classifies the entire scene as sea ice, therefore only the *Polar Ice Day* coverage subroutine is run. Again, $T_B(13.9\mu m)$ did not detect any clouds in the scene.

Figure 4.8(a) shows the original $T_B(3.9\mu m)$ - $T_B(11\mu m)$ test threshold. The original threshold detects much of the main cloud mass but subjective analysis suggests that this test is the reason why the original cloud mask is having difficulties with the thin cloud edges. Figure 4.8(b) shows the NPS $T_B(3.9\mu m)$ - $T_B(11\mu m)$ test threshold. The NPS threshold is detecting the thin clouds that were missed by the original threshold. It has also detected two smaller clouds along the bottom right of the scene. Although this is a daytime case and these two clouds are in shadow, the emittance difference between

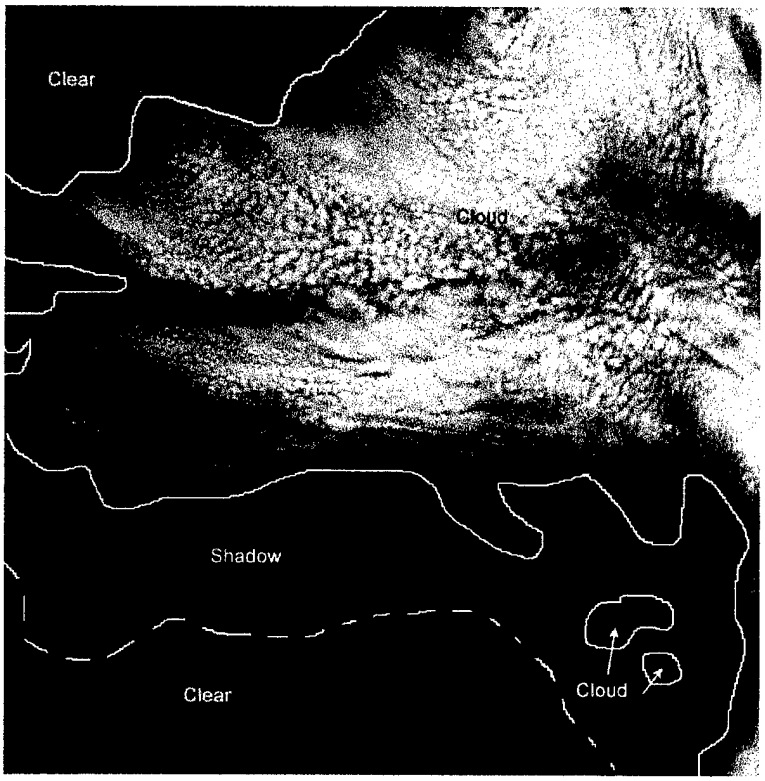

Figure 4.6. MAS FIRE/ACE Flight #98-68, Track 16, Center Time 23:31:38 UTC, is displayed as an RGB image where Red is band 20, Green is band 10, Blue is band 2. The scene contains both sea ice and high clouds, with clouds casting a shadow over the sea ice.

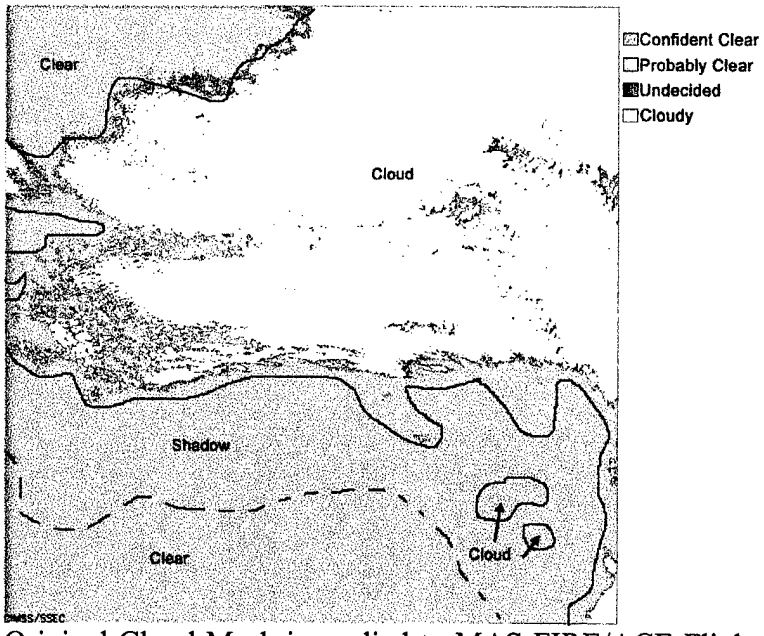

Figure 4.7. Original Cloud Mask is applied to MAS FIRE/ACE Flight #98-68, Track 16, Center Time 23:31:38 UTC, Mask classifications are described in the legend.

$T_B(3.9\mu m)$ and $T_B(11\mu m)$ still reveals the presence of the clouds. Again, noise is introduced into the test by the MAS IR bands.

Figure 4.9 shows the NPS cloud mask for this case. It detects the thin clouds along the edge of main cloud mass due directly to the threshold modifications in the $T_B(3.9\mu m)$ - $T_B(11\mu m)$ test. It also detects the two smaller clouds along the bottom right. Noise in the cloud mask is generated by the $T_B(3.9\mu m)$ - $T_B(11\mu m)$ test.

C. MAS FIRE/ACE FLIGHT #98-68, TRACK 4, CENTER TIME 20:11:05 UTC

MAS FIRE/ACE Flight #98-68, Track 4, Center Time 20:11:05 UTC, is a difficult case because sea ice is visible through semi-transparent clouds. The case is shown in Figure 4.10 where an optically thick cloud is casting a shadow on the clouds below it. Gravity waves are detectable in the thin, low-level clouds. $T_B(13.9\mu m)$ detected very little cloud and was not a factor in the ultimate confidence determination.

Figure 4.11 shows the original cloud mask. It classifies much of the scene as *Cloudy* or *Undecided.* It also classifies a portion of the shadow and the lower right corner of the scene as *Confident Clear.*

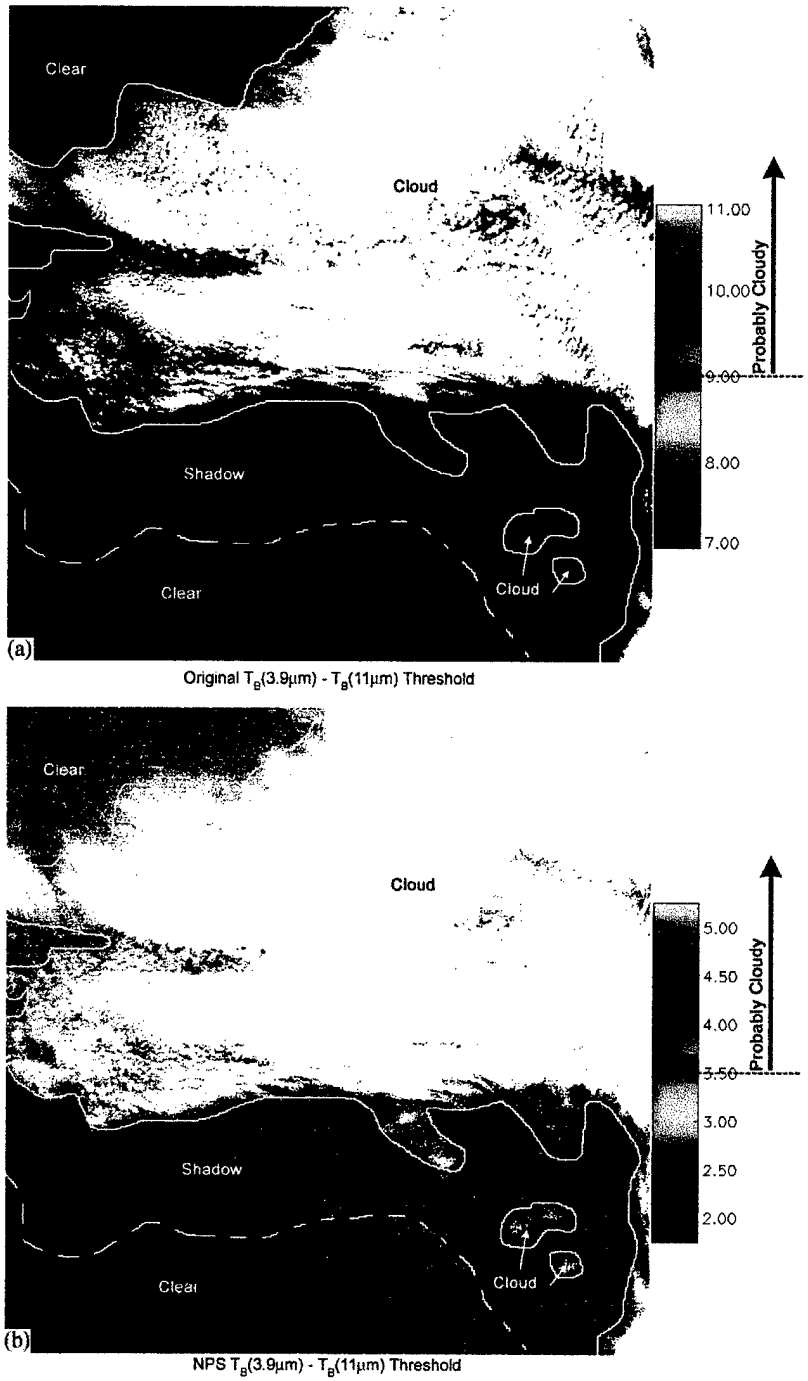

Figure 4.8. Original $T_B(3.9\mu m) - T_B(11\mu m)$ test threshold (a) and the NPS $T_B(3.9\mu m) - T_B(11\mu m)$ test threshold (b) are applied to MAS FIRE/ACE Flight #98-68, Track 16, Center Time 23:31:38 UTC. The figures are colored according to the thresholds set for each test. The original threshold did not detect the thin clouds, while the NPS threshold improved the thin cloud detection.

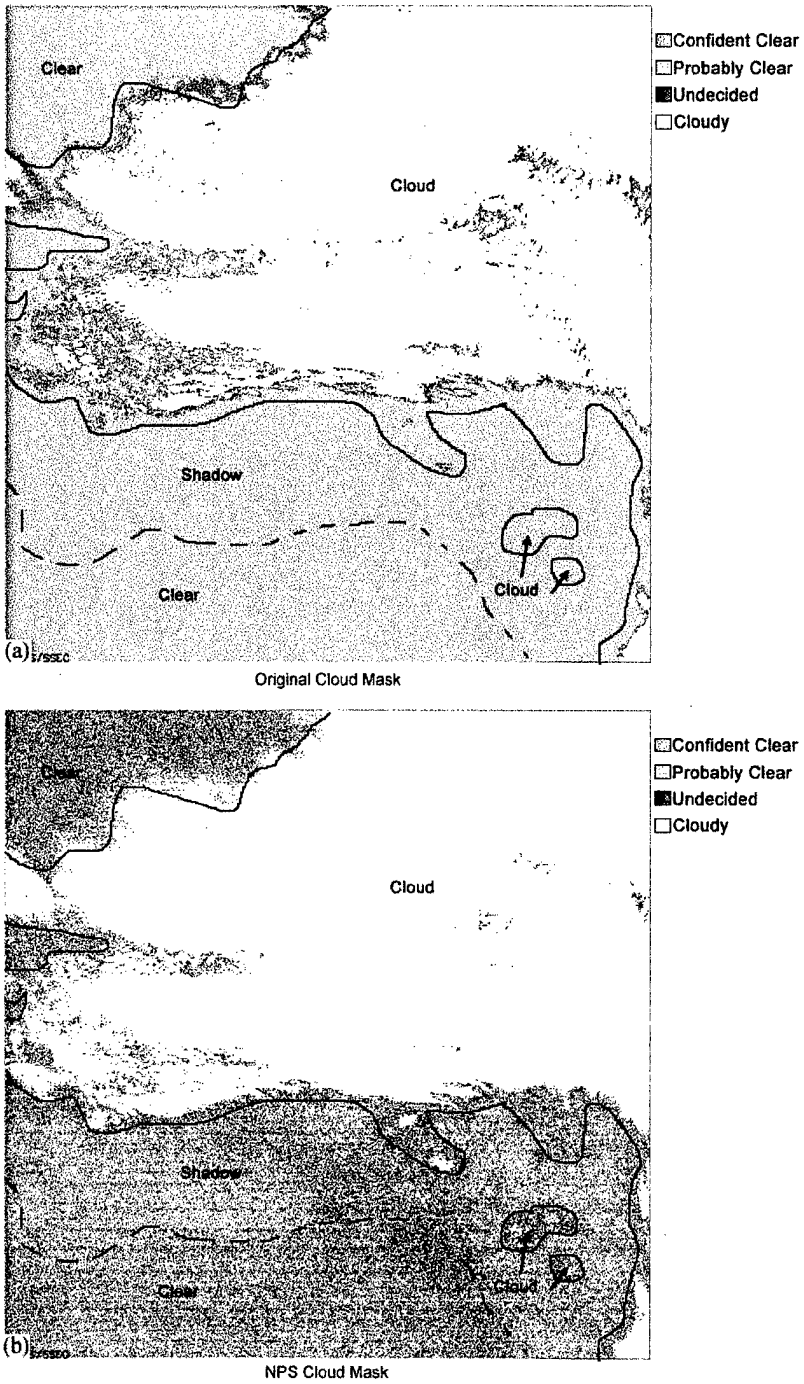

Figure 4.9. Original cloud mask (a) and the NPS cloud mask (b) are applied to MAS FIRE/ACE Flight #98-68, Track 16, Center Time 23:31:38 UTC. Mask classifications are described in the legend. (b) NPS Cloud Mask. The NPS cloud mask improved the detection of thin clouds.

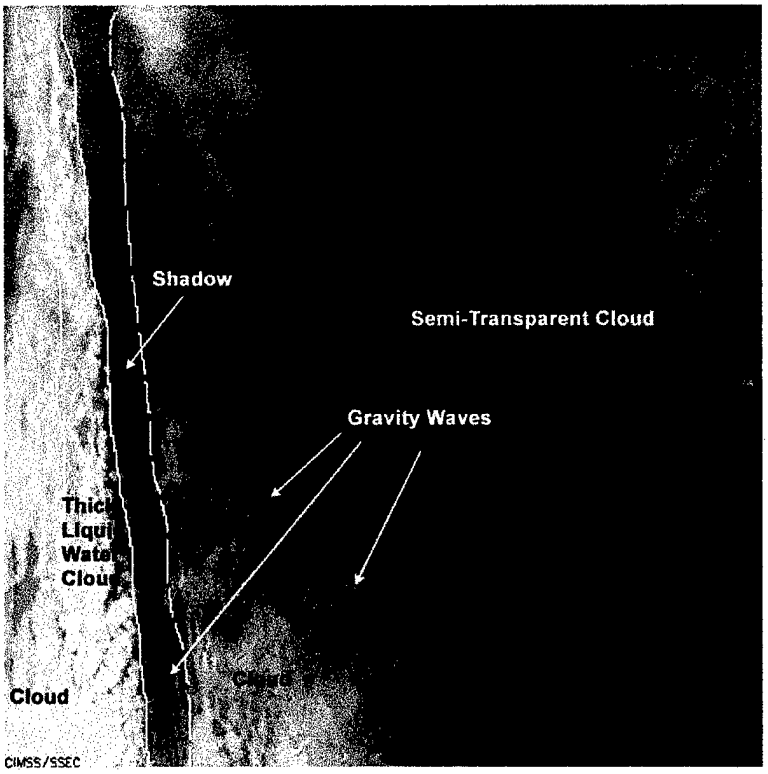

Figure 4.10. MAS FIRE/ACE Flight #98-68, Track 4, Center Time 20:11:05 UTC, is displayed as an RGB image where Red is band 20, Green is band 10, Blue is band 2. Optically thick cloud is casting a shadow on the clouds below it. Sea ice is visible through semi-transparent clouds and gravity waves are detectable in the thin, low-level clouds

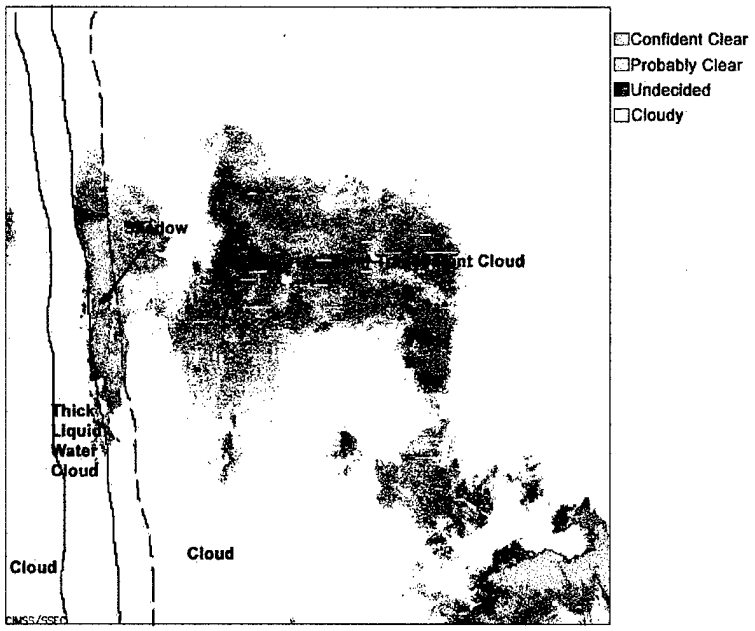

Figure 4.11. Original Cloud Mask is applied to MAS FIRE/ACE Flight #98-68, Track 4, Center Time 20:11:05 UTC. Mask classifications are described in the legend. Much of the scene as classified as *Cloudy* or *Undecided.* A portion of the shadow as classified *Confident Clear.* The lower right corner of the scene, the cloud mask identifies the area as *Confident Clear.*

Figure 4.12 shows where the Hall Test identifies sea ice. The pack ice in the scene and much of the multiyear ice floating in the open water is classified as sea ice. The test did not classify much of the optically thick cloud as sea ice.

Figure 4.13 shows the $T_B(3.9\mu m)$ - $T_B(11\mu m)$ difference. Semi-transparent low-level clouds and gravity waves are resolved. The test also resolves the shadow from the thick liquid water cloud.

When the Hall Test classifies the pixel as sea ice, the *Polar Ice Day* coverage is used. Figure 4.14(a) depicts the original $T_B(3.9\mu m) - T_B(11\mu m)$ test threshold. The test classifies the shadow area and much of the low level clouds as clear. The original test

resolves portions of the gravity waves in the low level clouds but the differences do not exceed the threshold necessary to classify the entire region as cloudy.

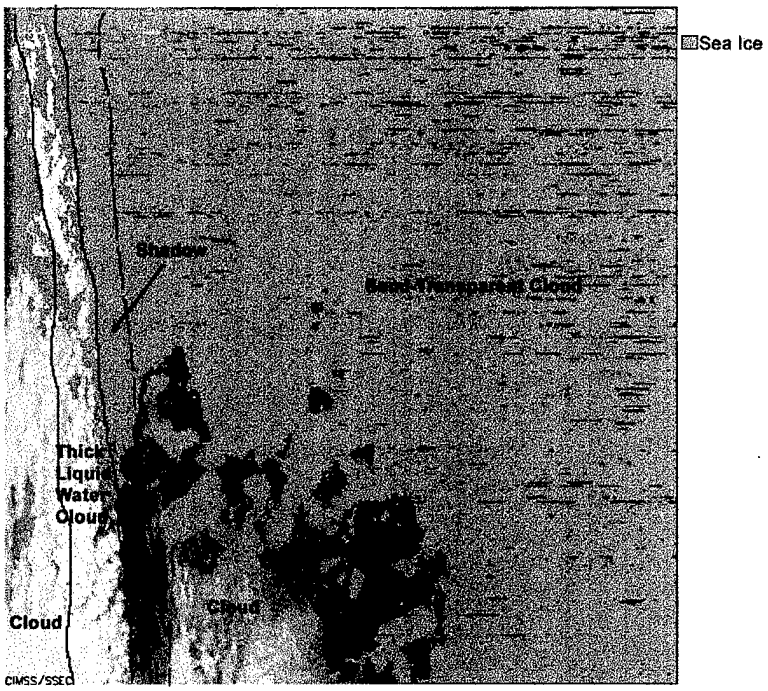

Figure 4.12. MAS FIRE/ACE Flight #98-68, Track 4, Center Time 20:11:05 UTC, Hall Test overlaid on a RGB image. The pack ice in the scene and much of the multiyear ice floating in the open water is classified as sea ice. The test did not classify much of the optically thick cloud as sea ice.

Figure 4.14(b) shows the NPS $T_B(3.9\mu m) - T_B(11\mu m)$ test threshold. The test now correctly classifies the shadow area as cloud. Much of the low level clouds that were missed by the original threshold are now identified as cloud. Finally, the gravity wave features are fully resolved by the test.

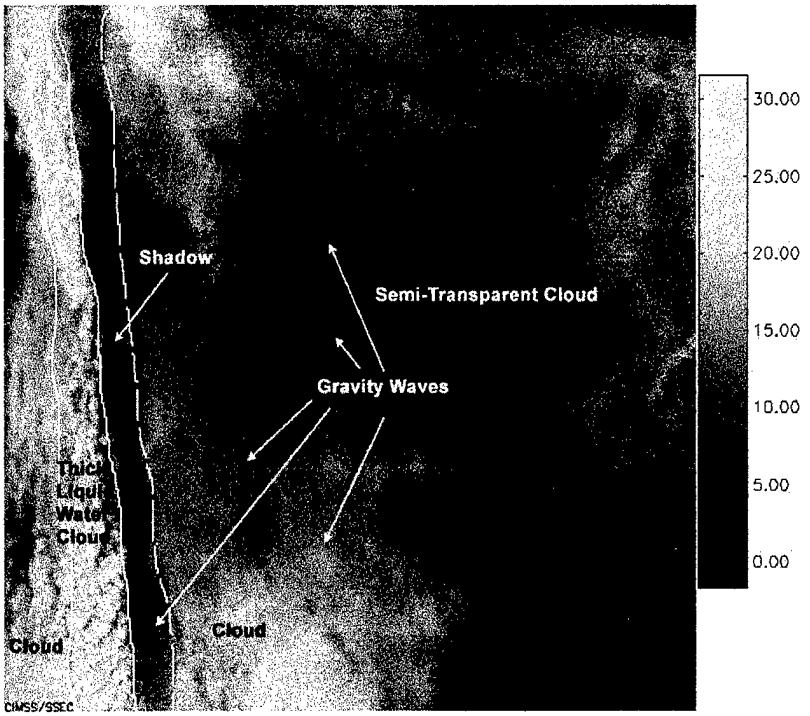

Figure 4.13. $T_B(3.9\mu m)$ - $T_B(11\mu m)$ difference applied to MAS FIRE/ACE Flight #98-68, Track 4, Center Time 20:11:05 UTC. The color scale on the right is the range of temperatures found in this scene. Semi-transparent low-level clouds and gravity waves are resolved. The test also resolves the shadow from the thick liquid water cloud.

Another *Polar Ocean Day* test is $T_B(11\mu m)$. Figure 4.15(a) shows the original $T_B(11\mu m)$ test threshold. The test correctly classifies the scene as cloudy. It has no trouble in the shadow area classifying it as cloud. Figure 4.15(b) shows the NPS $T_B(11\mu m)$ test threshold. It raises the clear confidence level where thin clouds are present over the sea ice but not to a level where it might be classified as *Confident Clear*.

Figure 4.16 shows the original and NPS cloud mask. The NPS cloud mask correctly classifies the shadow due to the threshold modifications in the $T_B(11\mu m)$ and $T_B(3.9\mu m)$ - $T_B(11\mu m)$ tests. The low-level clouds are also correctly classified as *Cloudy* due to the modification in the $T_B(3.9\mu m)$ - $T_B(11\mu m)$ test.

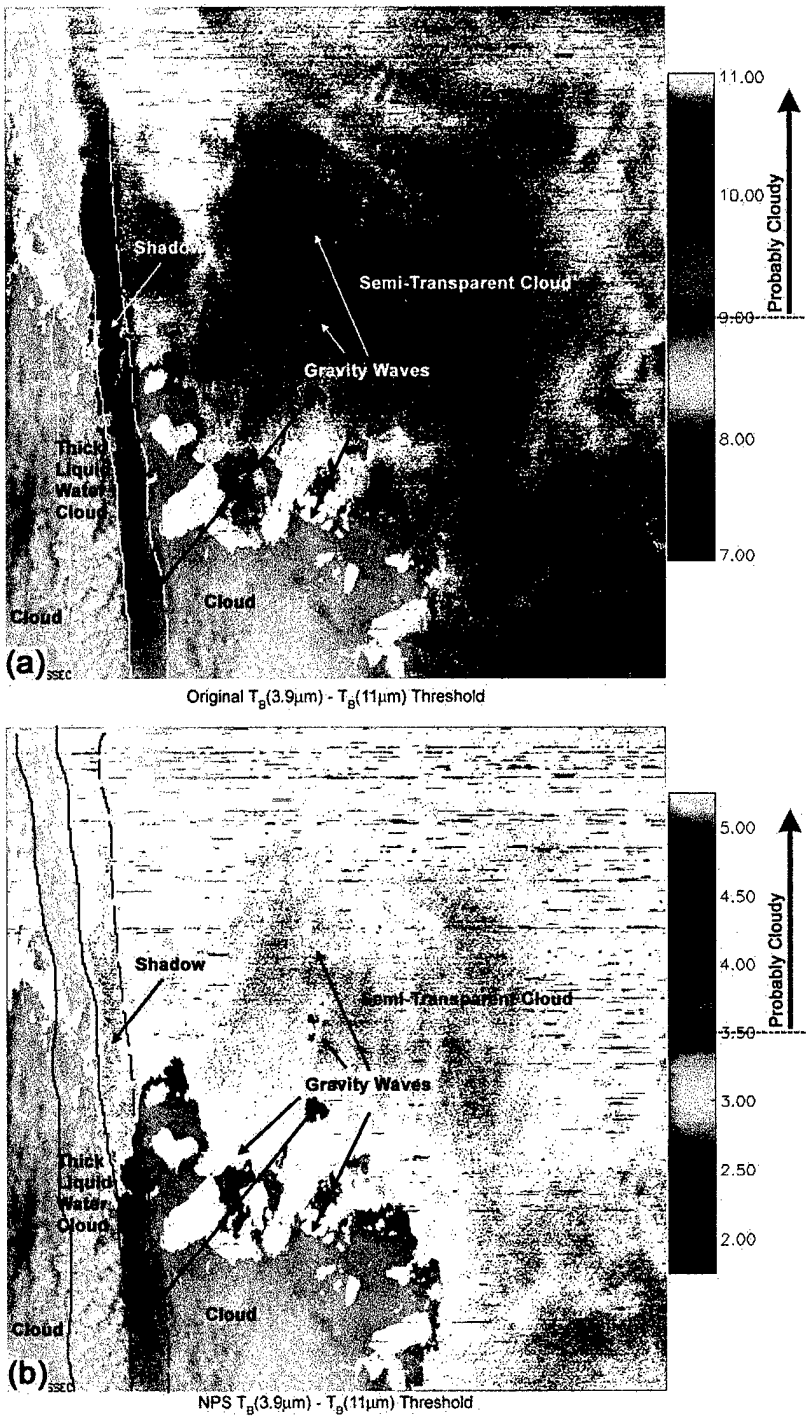

Figure 4.14. Original $T_B(3.9\mu m) - T_B(11\mu m)$ test threshold (a) and the NPS $T_B(3.9\mu m) - T_B(11\mu m)$ test threshold (b) are applied to MAS FIRE/ACE Flight #98-68, Track 4, Center Time 20:11:05 UTC and overlaid on $T_B(3.9\mu m) - T_B(11\mu m)$ difference. The figures are colored according to the thresholds set for each test. The original threshold classifies the shadow area and much of the low-level clouds as clear. The NPS threshold correctly classifies the shadow and low-level clouds as clouds

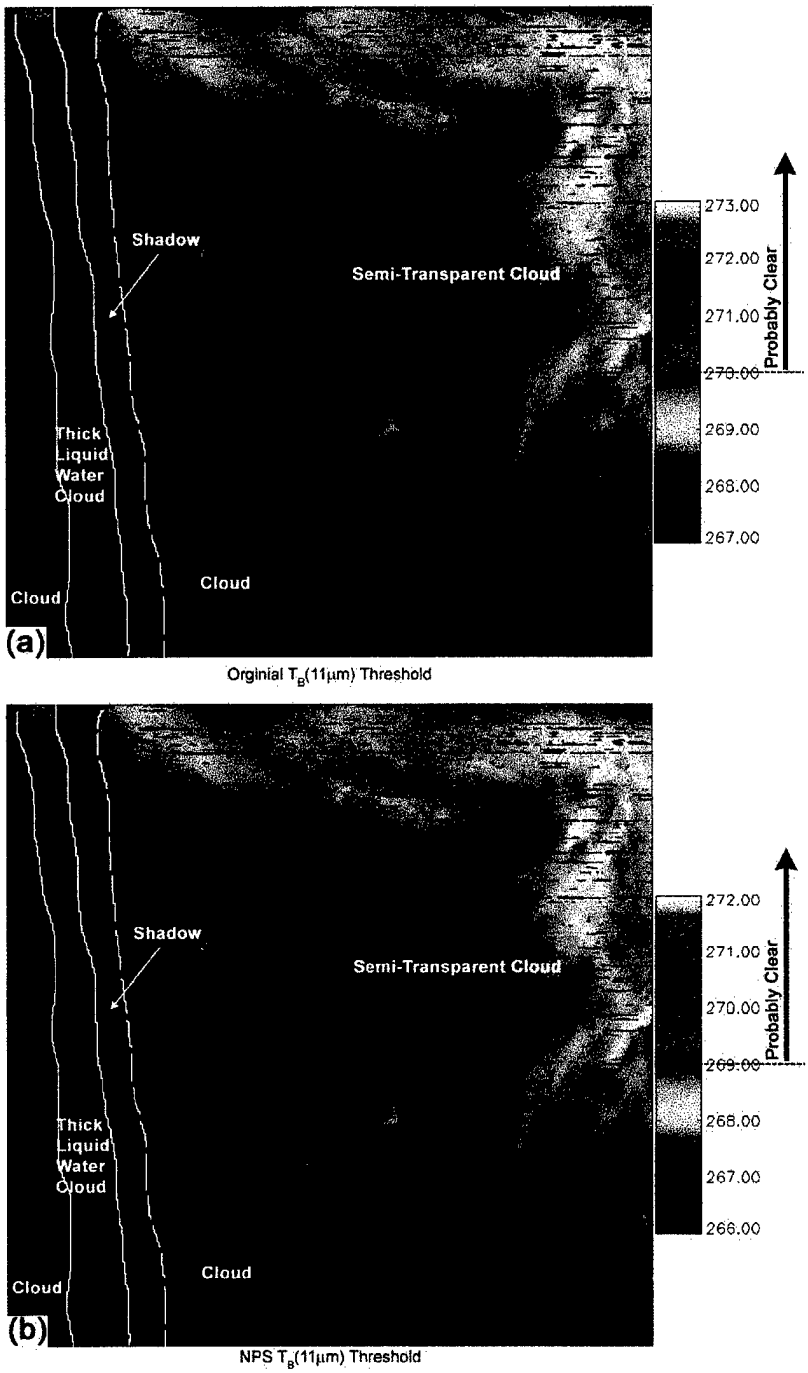

Figure 4.15. Original T_B(11μm) test threshold (a) and the NPS (11μm) test threshold (b) are applied to MAS FIRE/ACE Flight #98-68, Track 4, Center Time 20:11:05 UTC and overlaid on T_B(11μm). The figures are colored according to the thresholds set for each test.. Both tests classify the scene as generally cloudy.

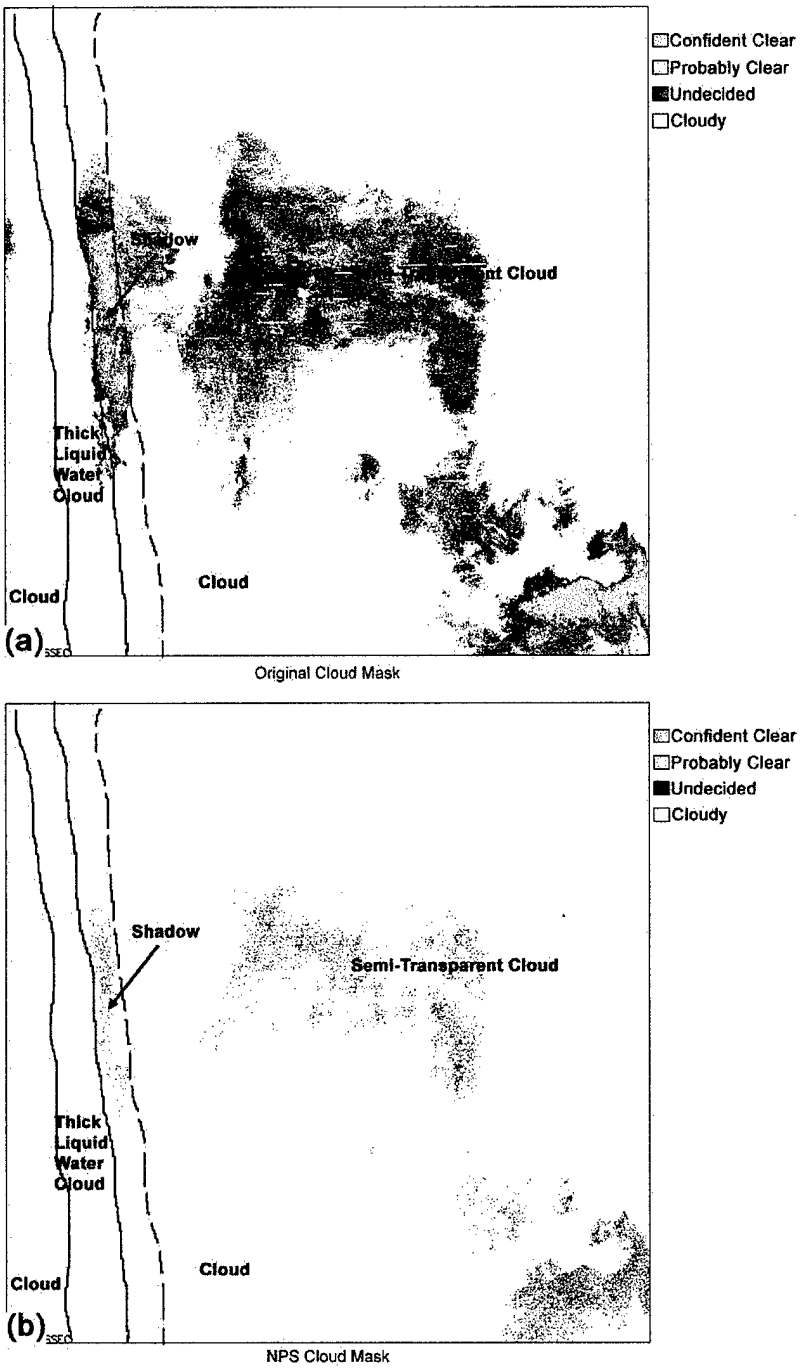

Figure 4.16. Original cloud mask (a) and the NPS cloud mask (b) are applied to MAS FIRE/ACE Flight #98-68, Track 4, Center Time 20:11:05 UTC. Mask classifications are described in the legend. The NPS cloud mask correctly classifies the shadow and low-level clouds as *Cloudy*.

D. MAS WINCE FLIGHT #97-45, TRACK 6, CENTER TIME 20:18:05 UTC

Figure 4.17 shows the ground track for Flight #97-45 conducted on February 6, 1997. This flight in not in a polar ocean region but has lake ice and is in the area of responsibility of the NIC.

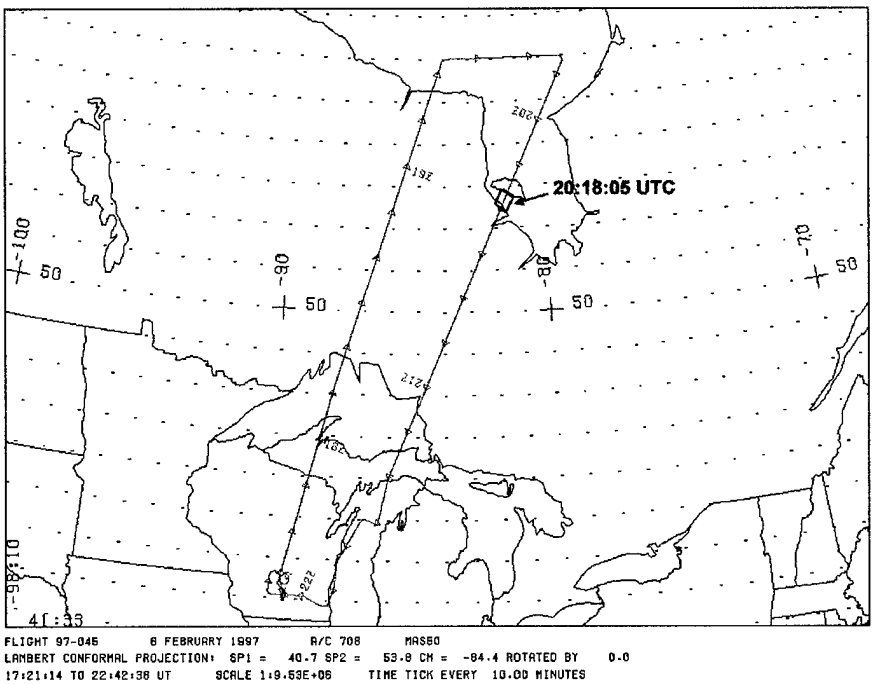

Figure 4.17. MAS WINCE Flight #97-45, Flight Track. (Gumley, 2000)

Figure 4.18 shows an RGB image of MAS WINCE Flight #97-45, track 6, with a center time of 20:18:05 UTC. It is in James Bay between the coast and Akimiski Island. There is fast ice along the shoreline with a large floe in the center of the scene. Leads are located between the fast ice and the floe where no sea ice is apparent. Small clouds are casting elongated shadows on the sea ice due to the high solar zenith angle of 75.2°.

The Hall Test classified the entire scene as either sea ice or snow with the exception of small areas that correspond to visible clouds. This included the leads that

appear to be open water in the visible and the IR bands. Figure 4.19(a) shows the NDSI test. With the exception of a few small areas where clouds are present, the NDSI value of the entire scene is greater than 0.4 and is therefore possibly sea ice or snow over land.

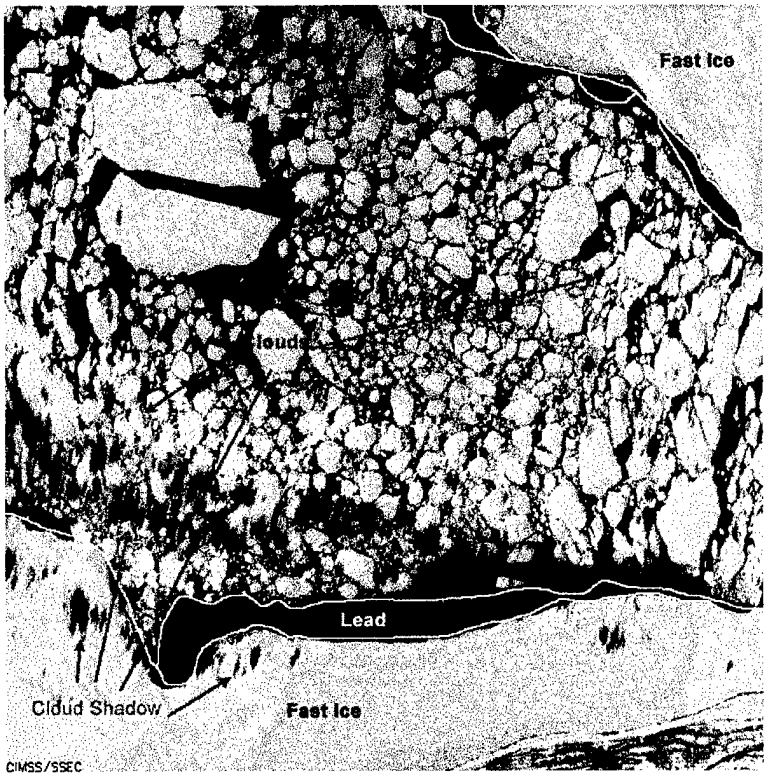

Figure 4.18 MAS WINCE Flight #97-45, Track 6, Center Time 20:18:05 UTC is displayed as an RGB image where Red is band 20, Green is band 10, Blue is band 2. Fast ice located along the shoreline with a large floe in the center of the scene. Leads are located between the fast ice and the floe where no sea ice is apparent. Small clouds are casting elongated shadows on the sea ice

Figure 4.19(b) shows $\rho_{0.88\mu m}$ for this scene. The entire scene may contain either snow or sea ice because no $\rho_{0.88\mu m}$ value was less than 0.1. In the leads, where $\rho_{0.88\mu m}$ is expected to be less than 0.1, there were no values less than 0.12. This may be due to a thin sheet of ice in the leads that is thin enough to be transparent at visible wavelengths but increases $\rho_{0.88\mu m}$ enough to pass the test for sea ice.

Figure 4.20 shows the original cloud mask. It correctly identifies much of the scene as *Confident Clear*. The clouds were detected, but a subjective analysis suggests that the cloud mask could do a better job in depicting the size and shape of the clouds. With the lead classified as sea ice, the cloud mask correctly identifies it as *Confident Clear*.

Figure 4.21 shows the $T_B(3.9\mu m)$ - $T_B(11\mu m)$ difference. This reveals the low level clouds in the scene. Figure 4.22(a) shows the original threshold as applied to the $T_B(3.9\mu m)$ - $T_B(11\mu m)$ test. The original threshold detects some of the clouds. Figure 4.22(b) shows the NPS threshold applied to the $T_B(3.9\mu m)$ - $T_B(11\mu m)$ test . Subjective analysis reveals that the NPS $T_B(3.9\mu m)$ - $T_B(11\mu m)$ test threshold increases the area of cloud detection. The clouds are better defined and better match the shadows in Figure 4.18. When fast ice and sea ice are present, there is a decrease in the clear confidence level for this test. In leads, the test is negative, indicating that $T_B(11\mu m)$ is greater than $T_B(3.9\mu m)$, thus increasing the clear confidence level. Again, the MAS IR channels are noisy.

Figure 4.23 shows the original and the NPS cloud mask. The new threshold for the $T_B(3.9\mu m)$ - $T_B(11\mu m)$ test has increased the number of pixels classified as *Cloudy*. Many pixels are classified as *Undecided* due to the noise in the $T_B(3.9\mu m)$ - $T_B(11\mu m)$ test, but these pixels still generate a confidence level of greater then 0.85 clear confidence level.

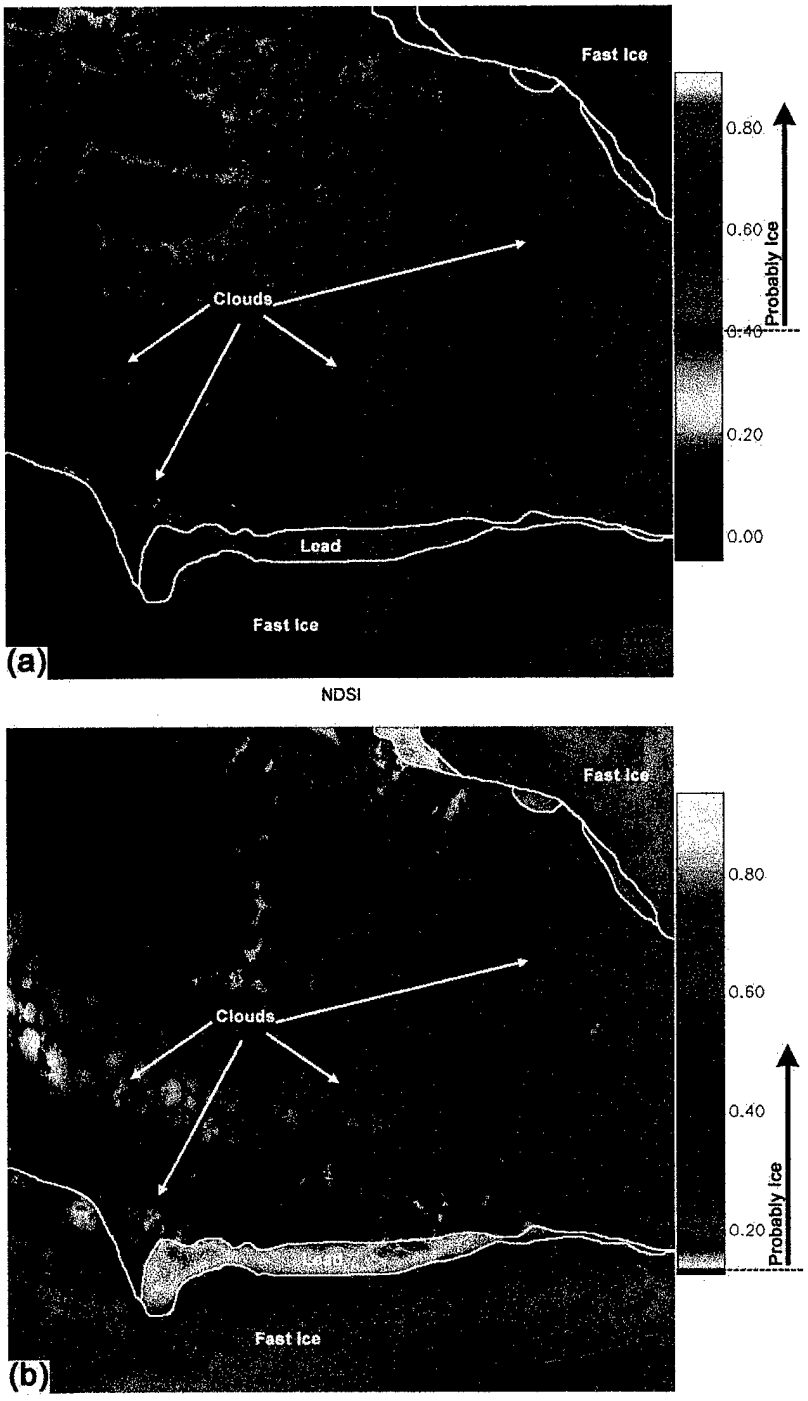

Figure 4.19 The NDSI test (a) and the $\rho_{0.88\mu m}$ test (b) is applied to MAS WINCE Flight #97-45, Track 6, Center Time 20:18:05 UTC. The figures are colored according to the thresholds set for each test. The NDSI test classifies pixels with values greater than 0.4 as *Probably Ice*. The $\rho_{0.88\mu m}$ classifies pixels with values greater than 0.1 as *Probably Ice*.

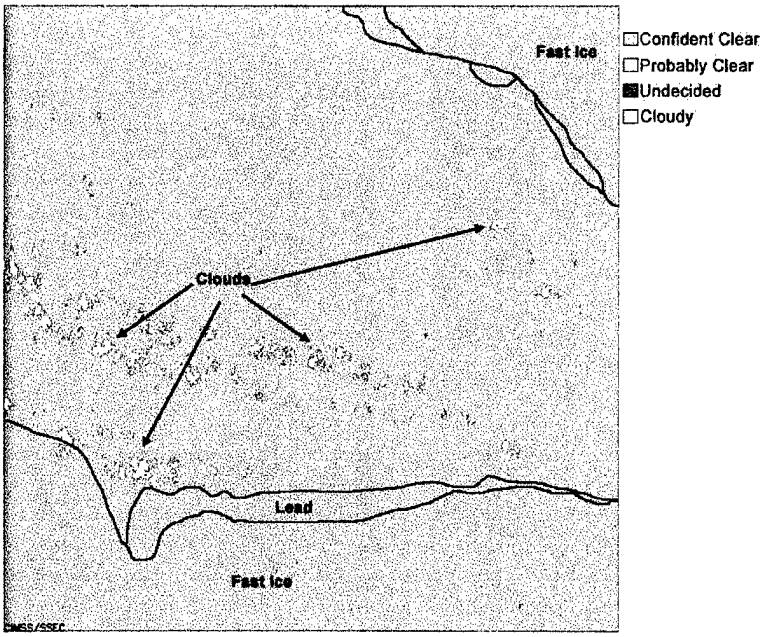

Figure 4.20 Original Cloud Mask is applied to MAS WINCE Flight #97-45, Track 6, Center Time 20:18:05 UTC. Mask classifications are described in the legend.

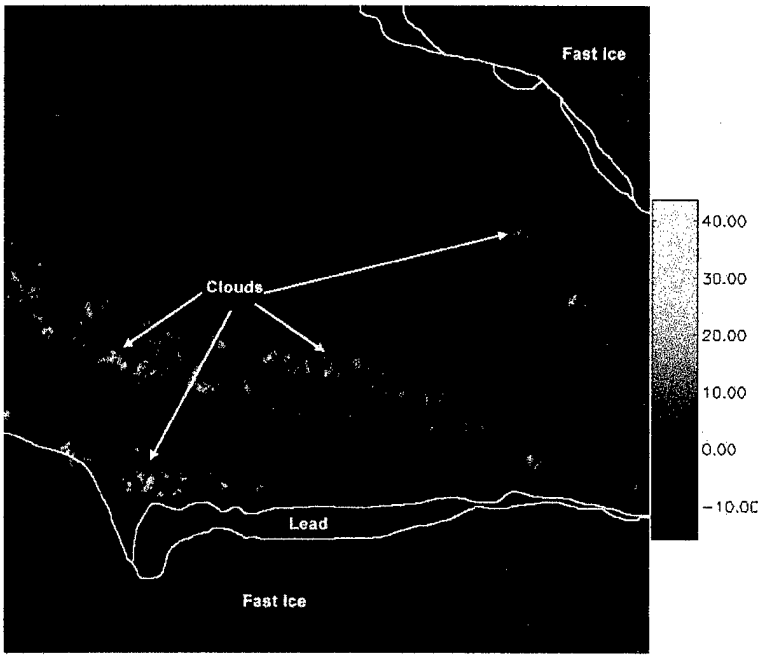

Figure 4.21 $T_B(3.9\mu m)$ - $T_B(11\mu m)$ difference applied to MAS WINCE Flight #97-45, Track 6, Center Time 20:18:05 UTC. The color scale on the right is the range of temperatures found in this scene.

E. STATISTICAL ANALYSIS

Table 4.1 shows the results of analyzing 18 tracks of data from three MAS flights. The average length of these tracks was 350 km and covered and average area of about 13,000 km^2. The NPS cloud mask classified 12.1% more pixels as *Cloudy* than the original mask. Subjective analysis of these tracks confirms that the new *Cloudy* pixels were indeed consistent with cloud features and not due to erroneous classification. *Confident Clear* pixels decreased by 35.2% in the NPS cloud mask indicating far fewer pixels are incorrectly identified as cloud-free. The NPS cloud mask generated about twice as many *Probably Clear* and *Undecided* pixels as the original cloud mask due to greater sensitivity to small, thin cloud features.

Table 4.1 Statistical summary of original and NPS cloud mask pixel classification.

	Original Cloud Mask	**NPS Cloud Mask**	**Change**
Total Pixels	92388744	92388744	
% *Confident Clear*	39781316 (43.0%)	25769650 (27.9%)	-14011666 (-35.2%)
% *Probably Clear*	1276156 (1.4%)	2444210 (2.6%)	1168054 (91.5%)
% *Undecided*	4039600 (4.4%)	9200997 (10.0%)	5161397 (127.8%)
% *Cloudy*	47291672 (51.2%)	54973887 (59.5%)	5512242 (12.1%)

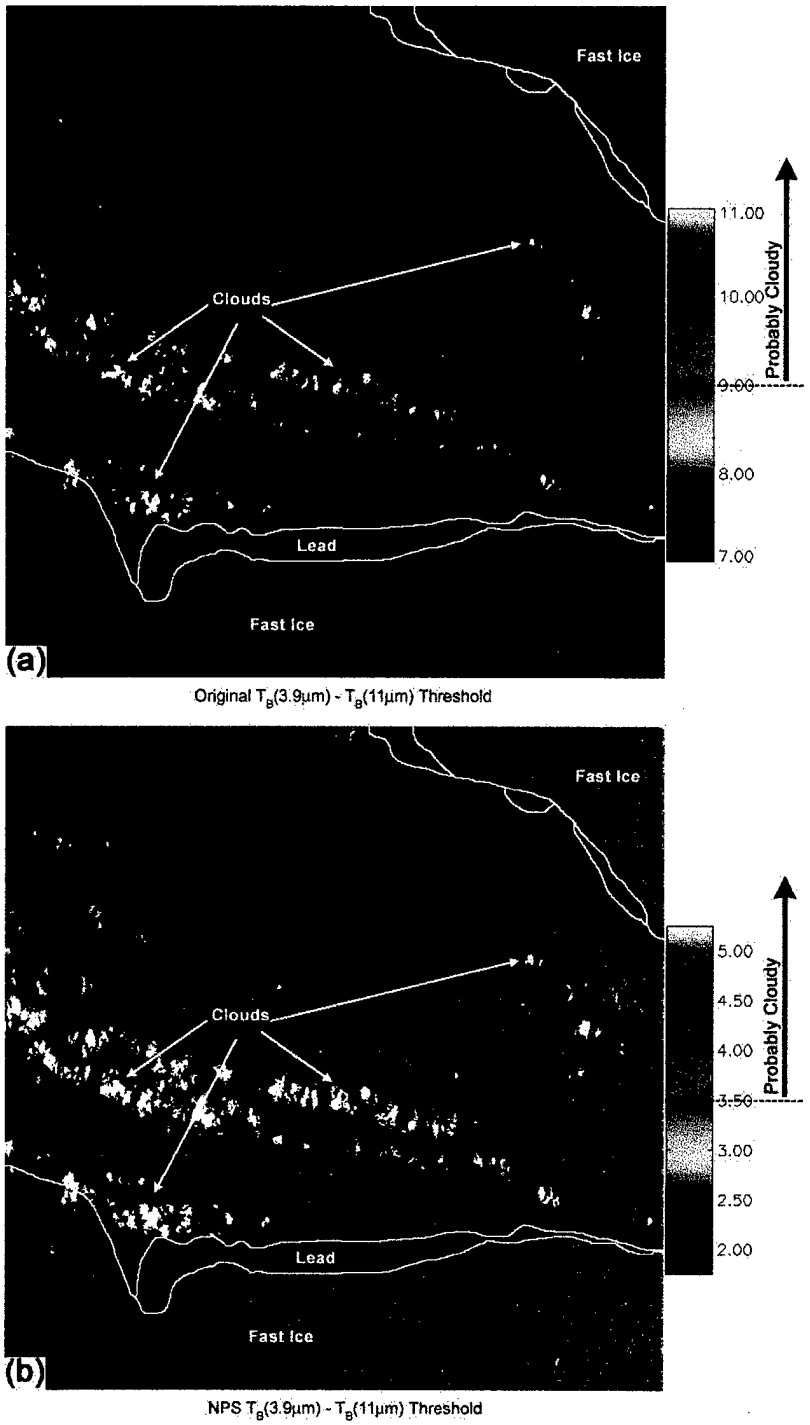

Figure 4.22 Original $T_B(3.9\mu m) - T_B(11\mu m)$ test threshold (a) and the NPS $T_B(3.9\mu m) - T_B(11\mu m)$ test threshold (b) are applied to MAS WINCE Flight #97-45, Track 6, Center Time 20:18:05 UTC. The original threshold detects some of the clouds. The NPS threshold increases the area of cloud detection and they are better defined

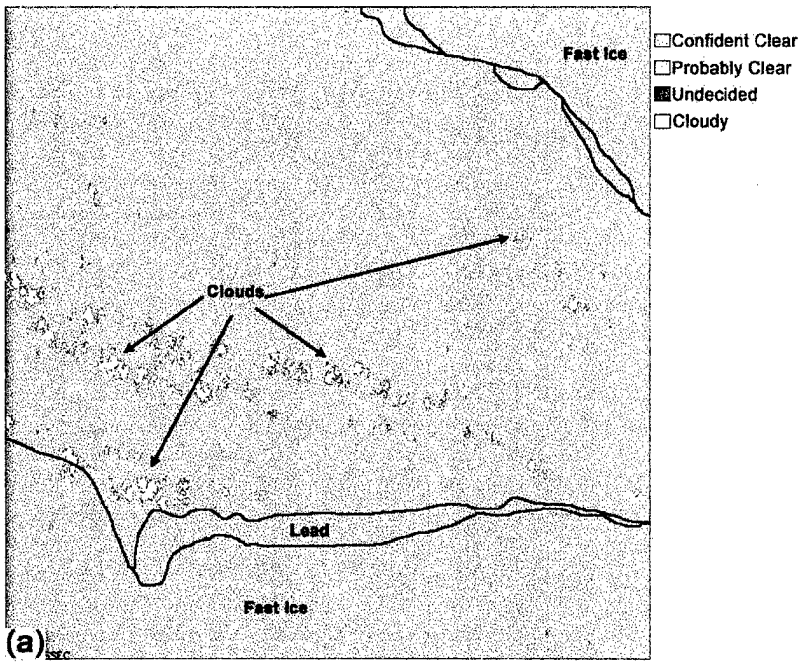

Original Cloud Mask

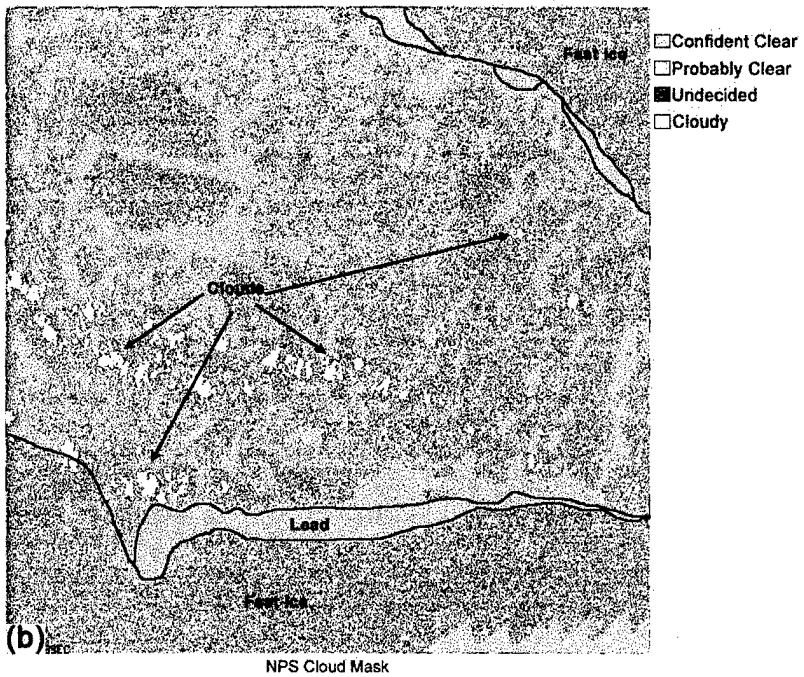

NPS Cloud Mask

Figure 4.23. Original cloud mask (a) and the NPS cloud mask (b) are applied to MAS WINCE Flight #97-45, Track 6, Center Time 20:18:05 UTC. Mask classifications are described in the legend.

THIS PAGE INTENTIONALLY LEFT BLANK

V. MODIS DATA

Figure 5.1 shows Terra's eastern Arctic ground track for April 1, 2000. Granule 17:00 UTC is a descending, daytime, track and is used to test the two new scene types on MODIS data.

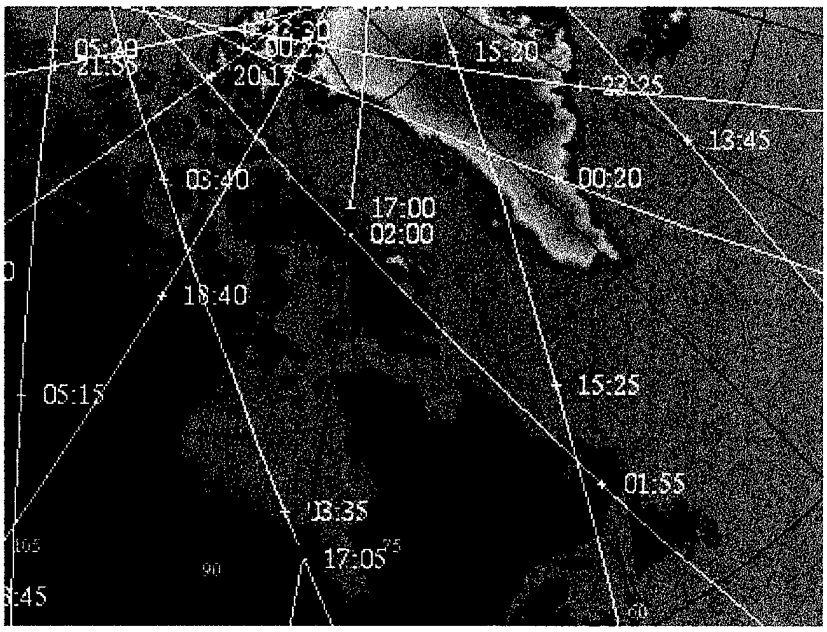

Figure 5.1. Terra's eastern Arctic ground tacks for April 1, 2000 (SSEC, 2000).

A. CALIBRATION ISSUES

There are calibration problems with some of the bands on the MODIS instrument and are believed to be correctable. Calibration problems with only the bands that affect the two new scene types are discussed below.

1. Band 26 (1.38μm)

The objective of Band 26 (1.38μm) is to detect high cirrus clouds. Unfortunately, there is electronic cross talk with Band 26 and bands that see the surface. This allows surface emittance to contaminate the reflectance value for Band 26.

2. Band 31 (11μm)

Band 31 (11μm) has optical cross talk contamination and is on the same focal plane as Bands 32 - 36. After 11μm energy passes through the filter, some of the energy does not reach the detector but remains in the substrate and contaminates the remaining Bands.

3. Band 35 (13.9μm)

Band 35 (13.9μm) has a scan mirror angle problem. Figure 5.2 is a graphic illustrating the scan mirror contamination. As the scan moves from left to right, there is an unexpected increase in the scan mirror angle. This leads to emittance from the scan mirror that increases the radiance value for Band 35. Therefore, an error is induced in T_B(13.9μm) as the scan mirror tracks from left to right from a correct value to a warmer value.

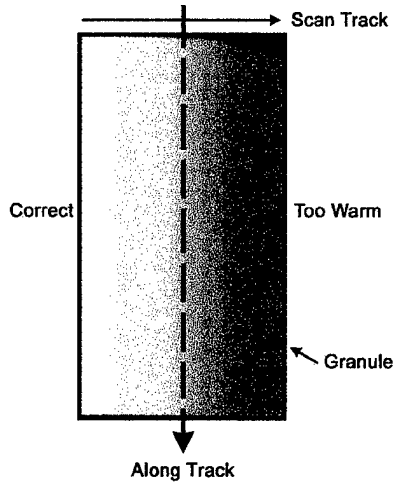

Figure 5.2. Band 35 (13.9μm) Scan Mirror Error. As the scan mirror tracks left to right, the mirror angle increases, which increases the brightness temperature across the scan.

B. HUDSON BAY

Figure 5.3 shows the April 1, 2000, 17:00 UTC, MODIS granule of the Hudson Bay. Figure 5.3(a) shows Band 2 (0.865μm) and Figure 5.3(b) shows Band 31 (11μm). Hudson Bay is mainly cloud free with first year sea ice dominating the entire bay. Mid to low-level clouds are present along the west coast of the bay and extending northeastward between Coats and Mansel Islands. Finally, high clouds cover the Foxe Basin to the north and James Bay to the south.

Figure 5.4 shows the $T_B(11\mu m)$ test for the April 1, 2000, 17:00, UTC MODIS granule with a land mask applied to highlight the water areas. Figure 5.4(a) shows the original threshold, while Figure 5.4(b) shows the NPS threshold. As described in Chapter III, the original MODIS $T_B(11\mu m)$ test threshold is too high for a polar ocean region. When the NPS threshold is applied to the MODIS $T_B(11\mu m)$ test, the clear confidence level for an individual pixel became more representative for a polar ocean scene.

At the location indicated by A in Figure 5.4, the NPS threshold improves the detection of the clear skies in the Davis Strait because the new threshold takes into account the lower surface temperatures associated with polar oceans. At B in Figure 5.4, the NPS threshold raises the clear confidence level over the sea ice in the Hudson Strait where some low and high clouds are present. Finally, at location C in Figure 5.4 the NPS threshold raises the clear confidence level over the sea ice where the low clouds are present. The increase in the clear confidence level at locations B and C is not enough to incorrectly identify the locations as clear.

Figure 5.5 shows the $T_B(3.9\mu m)$ - $T_B(11\mu m)$ test for April 1, 2000, 17:00 UTC, MODIS granule. Again, Figure 5.5(a) shows the original threshold and Figure 5.5(b) shows the NPS threshold. As with the MODIS $T_B(11\mu m)$ test, the MODIS $T_B(3.9\mu m)$ - $T_B(11\mu m)$ test threshold is too high for a polar ocean region. Locations A and D are regions where high clouds cover the surface. The NPS threshold lowered the clear confidence level for these regions enough for the high clouds to be classified correctly. For low clouds, locations B and C had the greatest improvements. The new threshold detected the low level cloud that was missed at B and increased the detection of low clouds at C.

Figure 5.6(a) shows the original cloud mask. It classifies portions of the clear area in the Davis Strait (A) as *Undecided* to *Confident Clear*. Figure 5.6(b) shows the NPS cloud mask correctly classifies location A as *Confident Clear*. This is a direct result of lowering the $T_B(11\mu m)$ test threshold. The NPS cloud mask also changed the classification of the clouds at location B so that almost all of the pixels are classified as *Cloudy*. At location C, where high clouds covered James Bay, the NPS cloud mask correctly increased the number of pixels classified as *Cloudy*. The changes at B and C were a direct result of lowering the $T_B(3.9\mu m)$ - $T_B(11\mu m)$ test threshold. The demarcation between *Undecided* and *Confident Clear* in the center of both cloud masks (under the label "Foxe Basin" and "Hudson Bay") is due to Band 35 scan mirror error.

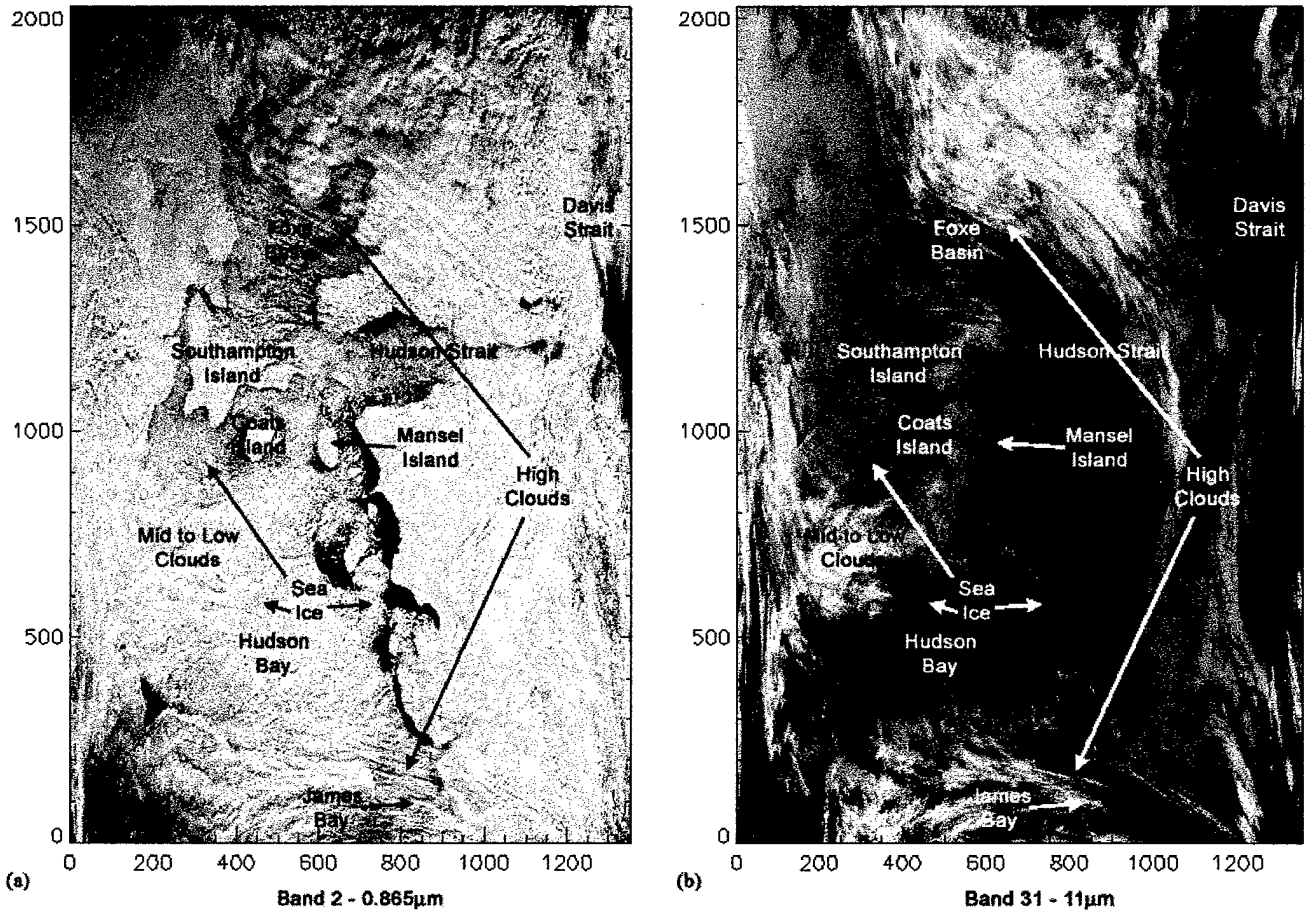

Figure 5.3. Band 2 (a) and Band 31 (b) for Hudson Bay, 1 April, 2000, MODIS 17:00 UTC granule. Hudson Bay is mainly cloud free with first year sea ice dominating the entire bay. Mid to low-clouds are present long the west coast of the bay and extending north eastward between Coats and Mansel Islands. Finally, high clouds cover the Foxe Basin to the north and James Bay to the south

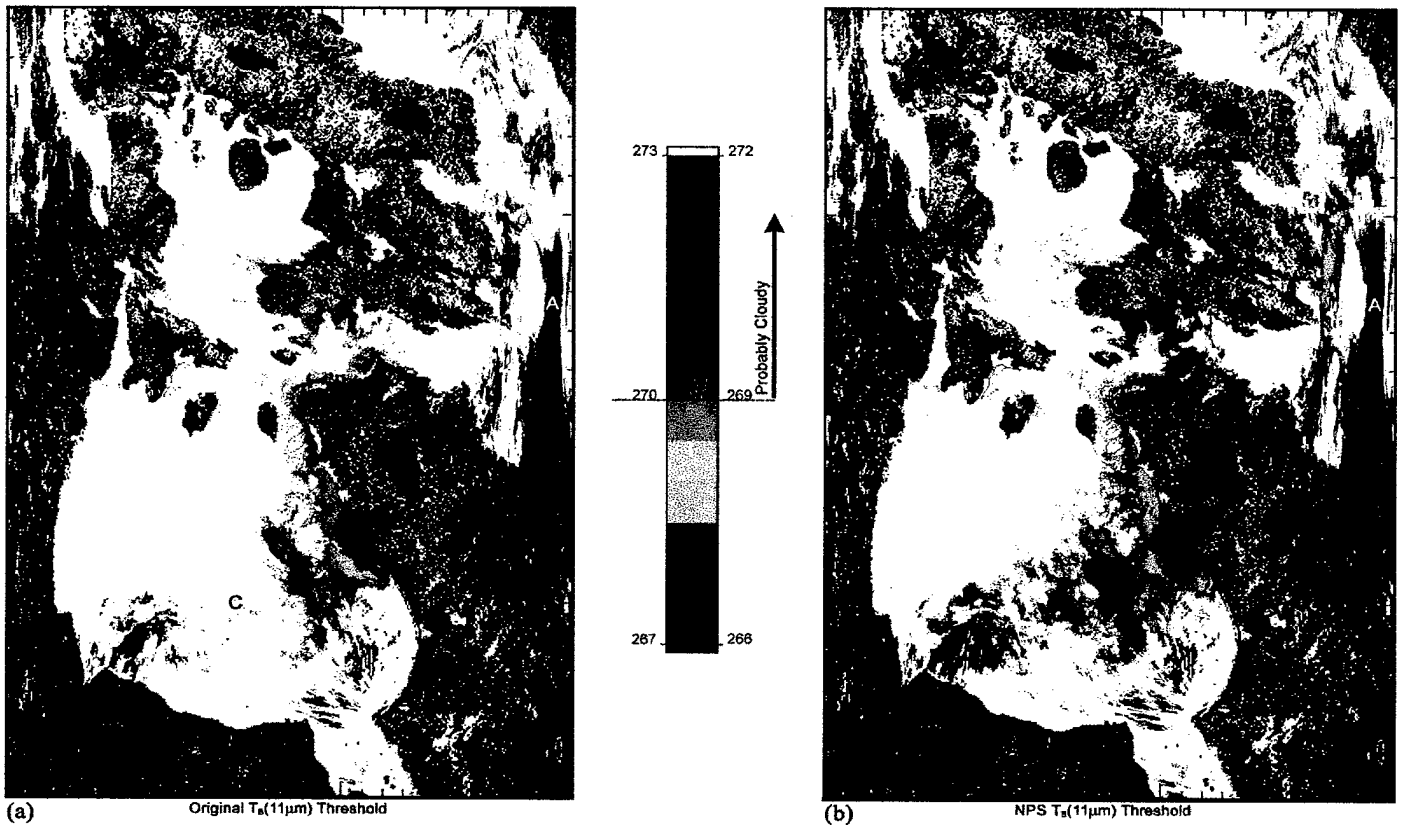

Figure 5.4. Original $T_B(11\mu m)$ test threshold (a) and the NPS $T_B(11\mu m)$ test threshold (b) are applied to Hudson Bay, April 1, 2000, MODIS 17:00 UTC granule. Color bar in the center are the thresholds for the two tests with β as midpoint. Brown indicates where the pixel's ecosystem was either coast or land and the NPS cloud mask as not applied.

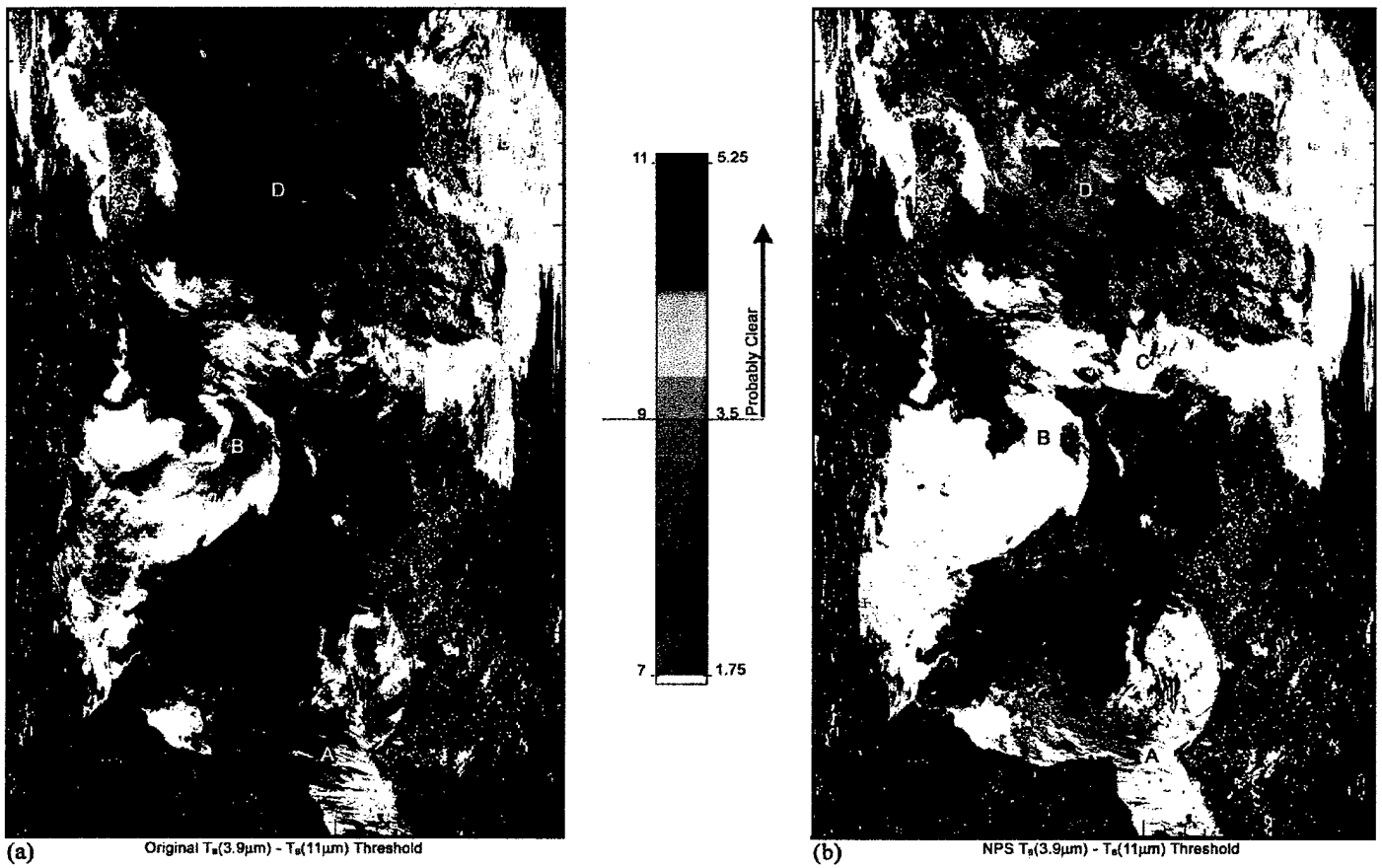

Figure 5.5. Original $T_B(3.9\mu m)$ - $T_B(11\mu m)$ test threshold (a) and the NPS $T_B(3.9\mu m)$ - $T_B(11\mu m)$ test threshold (b) are applied to Hudson Bay, April 1, 2000, MODIS 17:00 UTC granule. Color bar in the center are the thresholds for the two tests with β as midpoint. Brown indicates where the pixel's ecosystem was either coast or land and the NPS cloud mask as not applied

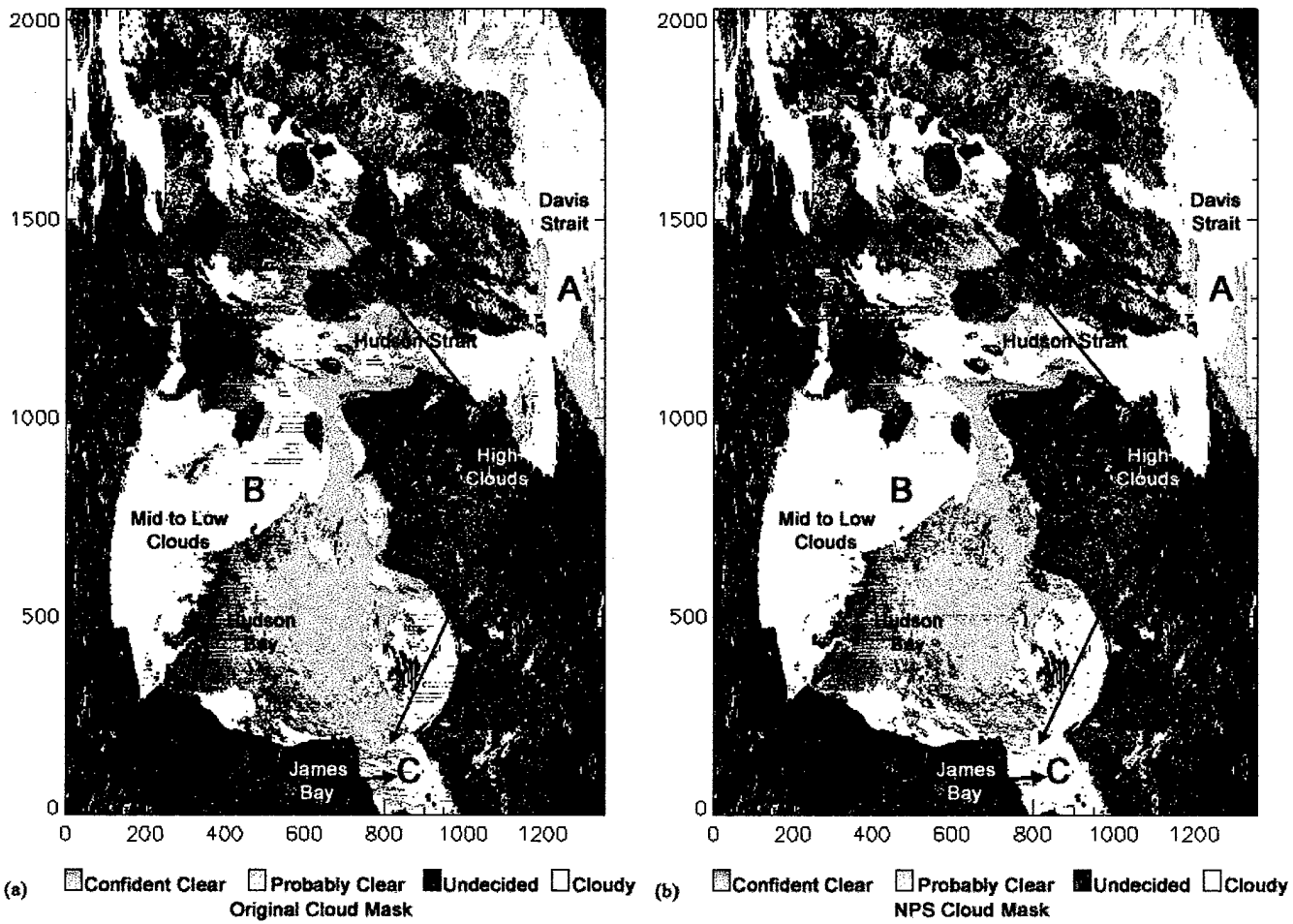

Figure 5.6. Original cloud mask (a) and the NPS cloud mask (b) are applied to Hudson Bay, April 1, 2000, MODIS 17:00 UTC granule. Mask classifications are described in the legend.

CONCLUSIONS AND RECOMMENDATIONS

A. CONCLUSIONS

Initial optimization of the MODIS cloud mask for the polar ocean regions is described based on 8 daytime MAS flights. 18 tracks (approximately 350km x 36km) were selected from 3 of these flights that had the greatest scene variability. MAS flights revealed that daytime thresholds for $T_B(11\mu m)$ and $T_B(3.9\mu m) - T_B(11\mu m)$ tests are too high for the polar ocean regions and must be lowered to compensated for lower average surface temperatures. In addition, the $T_B(11\mu m) - T_B(12\mu m)$ test gives little useful information during the daytime. Finally, $T_B(13.9\mu m)$ test was never a factor in the cases examined in this study.

Because of the unique nature of the polar ocean regions, two new scene types were developed for the MODIS cloud mask. The new scene types incorporate new thresholds appropriate for polar ocean regions and are included in the NPS modified MAS/MODIS cloud mask (NPS cloud mask). The first new scene type is *Polar Ice Day* and is initiated during the day and when the pixel is identified as having sea ice. The second scene type is *Polar Ocean Day* and is initiated during the day and when the pixel is identified as water located greater than 60° north and south.

The modifications greatly improve the detection of clouds over cold polar oceans where sub-pixel sea ice may be present or water temperatures might falsely indicate clouds. The number of *Cloudy* pixels (≤ 0.66 clear confidence level) for a given scene was increased 12.1% on average for MAS cases. The NPS cloud mask also classified

two times more *Probably Clear* and *Undecided* pixels than the original mask due to greater sensitivity to thin, small clouds.

The improvements that were observed in the MAS data were confirmed when the NPS cloud mask was applied to 5 uncorrected MODIS cases. One case is presented here. The NPS cloud mask improved the clear confidence level when surface temperatures were below 273°K. It also lowered the clear confidence level when there were high and low clouds over the sea ice.

The NPS MODIS cloud mask that was derived from Ackerman et al. (1997) will provide the NIC with the means to assist its analysts by giving them a tool to correctly identify clouds that might have been misidentified as sea ice in the past. A better quality sea ice analysis will result. Ultimately, this cloud mask will also lay the foundation for the development of ice recognition algorithms.

B. RECOMMENDATIONS

The operational MODIS cloud mask must have new scene types that are optimized for the polar ocean regions. It is not appropriate for thresholds, set for the globe, to be applied to the polar oceans due to their distinctly different surface temperatures. Unfortunately, further work should not proceed until calibration is completed for the MODIS instrument. Once completed, the two new scene types must be tested on a larger daytime dataset consisting of Arctic and Antarctic granules. Finally, work needs to be done on thresholds for nighttime cases that were not possible for this thesis.

LIST OF REFERENCES

Acharya, P.K., D.C. Robertson, and A. Berk, 1993: Upgraded Line-of-Sight Geometry Package and Band Model Parameters for MODTRAN, Phillips Laboratory Technical Report PL-TR-93-2127, Geophysics Directorate, Hanscom AFB, MA.

Ackerman, S.A., K. I. Strabala, W. P. Menzel, R.A. Frey, C. C. Moeller, L. E. Gumley, 1998: Discriminating Clear Sky From Clouds With MODIS. *J. Geophys. Res.*, **103** , No. D24, 32141-32157.

Comiso, J.C., 1994: Surface Temperatures In The Polar Regions From Nimbus-7temperature Humidity Infrared Radiometer. *J. Geophys. Res.*, 99(C3), pp 5181-5200.

Gao, B.-C., Goetz, A. F. H., & Wiscombe, W. J. (1993). Cirrus Cloud Detection From Airborne Imaging Spectrometer Data using The 1.38 micron Water Vapor Band. *Geophysical Research Letters*, 20(4), 301-304.

Gumley, Liam E., Greg Cleven, Paul A. Hubanks, cited 2000: MODIA Airborne Simulator. [Available on-line from http://ltpwww.gsfc.nasa.gov/MODIS/MAS/Home.html].

Herring, David, cited 2000: Terra Mission Status. [Available on-line from http://terra.nasa.gov/Events/terramissionstatus.html].

Hook, S.J. and H. L. Tan, cited 2000: ASTER Home Page. [Available on-line from http://asterweb.jpl.nasa.gov].

Hutchison, K. D., and K. R. Hardy, 1995: Threshold Functions For Automated Cloud Analyses Of Global Meteorological Satellite Imagery. *Int. J. Remote Sens.*, **16**, 3665-3680.

National Aeronautics and Space Administration, 1999 Eos Reference Handbook; A Guide To Nasa's Earth Science Enterprise And The Earth Observing System, NASA/Goddard Space Flight Center, Greenbelt, M.D., 1999.

National Aeronautics and Space Administration, Terra: Flagship Of The Earth Observing System; Press Kit November *1999*, Release No. 99-120, NASA/Goddard Space Flight Center, Greenbelt, M.D., 1999a.

National Aeronautics and Space Administration, NASA's Earth Observing System, The First EOS Satellite, EOS AM-1, NASA/Goddard Space Flight Center, Greenbelt, M.D., 1999b.

National Aeronautics and Space Administration, Modis, Moderate Resolution Imaging Spectroradiometer, NASA/Goddard Space Flight Center, Greenbelt, M.D., 1999c.

INITIAL DISTRIBUTION LIST

1. Defense Technical Information Center 2
   8725 John J. Kingman Road, Suite 0944
   Ft. Belvoir, VA 22060-6218

2. Dudley Knox Library 2
   Naval Postgraduate School
   411 Dyer Road
   Monterey, CA 93943-5101

3. Cherly Bertoia 2
   National/Naval Ice Center
   Federal Building #4
   4251 Suitland Road
   Washington, DC 20395

4. Space Science and Engineering Center 1
   University of Wisconsin-Madison
   1225 W. Dayton St.
   Madison, WI 53719

5. LT Sean P. Memmen, USN 1
   632 Analii Street
   Diamondhead, MS 39525

6. Professor Philip A. Durkee, MR/De 2
   Naval Postgraduate School
   Monterey, CA 93943-5000

7. Professor Peter S. Guest, MR/Gs 1
   Naval Postgraduate School
   Monterey, CA 93943-5000

8. Chairman 2
   Department of Meteorology
   Naval Postgraduate School
   Monterey, CA 93943-5000

9. Robert L. Creasey, MR/Cr 1
   Naval Postgraduate School
   Monterey, CA 93943-5000